

David A. Stoney,¹ Ph.D., Andrew M. Bowen,² M.S., Vaughn M. Bryant,³ Ph.D., Emily A. Caven,² M.S., Matthew T. Cimino,² Ph.D. and Paul L. Stoney,² MBA

Particle Combination Analysis for Predictive Source Attribution: Tracing a Shipment of Contraband Ivory⁴

ABSTRACT

Dusts from within a shipment of contraband ivory were analyzed to help determine the original location where the ivory was packed. Key findings were the types of minerals, soil, and vegetation represented in the dust, as determined using a combination of light and electron microscopy, energy dispersive x-ray analysis, infrared microspectroscopy, palynology and non-human DNA analysis. Beginning with a possible origin within the continent of Africa, first-stage analysis of the recovered dusts was able to eliminate environments comprising approximately 91% of the area, including all areas of 36 countries. Of the remaining 12 countries, the analysis was able to eliminate 72% of their area, allowing the investigations to be focused within portions of these countries. Next steps were defined to further reduce the possible origins of the dust based on more detailed regional analyses.

INTRODUCTION

Fine dust particles, adhering to virtually any object and within virtually any product, are the result of a history of exposure. Routinely, such dusts contain a tremendous variety of particles, including those of mineral, botanical, zoological, microbial, and anthropogenic character. The large number of particles in these dusts, and their variety, provide an extremely rich source of potential information – translating into a powerful inferential tool – when the particles are appropriately analyzed and appropriately

¹ Corresponding author: Stoney Forensic, Inc., 14101-G Willard Road, Chantilly, VA 20151.

² Stoney Forensic, Inc., Chantilly, VA

³ Palynology Laboratory, Texas A&M University, College Station, TX.

⁴ Portions presented at the INTERPOL, 6th International Conference on Environmental Crime, Lyons, France, October 13–17, 2008 and the Society for Wildlife Forensic Sciences, Inaugural Meeting, Ashland, Oregon, April 19–23, 2010. Work on case-related law enforcement and forensic laboratory analyses has been presented at these conferences and at the NIJ/FBI Trace Evidence Symposium, Clearwater Beach, Florida, August 2–7, 2009 by Ken Goddard, Director of the US National Fish and Wildlife Forensics Laboratory.

interpreted. When faced with alternative hypothetical geographical, environmental, and human activity exposures, the results of fine dust analysis allow the exclusion of many sources of exposure, and the appraisal of others with degrees of support for hypotheses ranging from highly unlikely to strongly compelling. The results can be extremely useful and allow predictive source attribution. That is, they contain an intelligible "signal" regarding provenance: where items or people originated, how they have been transported, and the people, conditions and environments to which they have been exposed.

This use of fine dusts, extracting signals allowing predictive source attribution, is distinguished from, and complementary to, those trace evidence tasks addressing either (1) comparison with specific possible sources or (2) classification among a set of pre-defined sources. These distinctions result in different limitations and they enable solving different problems.

Comparison with specific possible sources

The task of comparison with specific possible sources (individualization by direct comparison) has a frequent application in the comparison of trace evidence found on a suspect with that found at a particular (typically crime scene) location. Published case reports of this type are common.[1] The focus is on the presence and variability of specific particle types. Two questions are of primary importance for this task

- Are the differences that are seen between the two samples sufficient to exclude a common origin?
- To what extent do the corresponding particle types, and their estimated frequencies of joint occurrence, support a hypothesis of common origin?

The purpose of comparison with specific possible sources is to rule out a specific source or to include it with a high degree of specificity. The specificity obtainable depends on the individuality of the features that are analyzed, compared and found to be in correspondence between the two samples.

To compare with specific possible sources, one must have "known" comparative reference samples from a location and one must apply an analytical protocol that is sensitive to highly individual sample characteristics. The analytical results from the reference samples are compared to those from the "questioned" sample (usually associated with a suspect). Based on the comparison, there is either a conclusion that the questioned sample is *not* from the same source as the reference sample, or that it *could be* from the same source (along with an estimate of the specificity of the conclusion). This approach is very appropriate for certain types of problems, but predictive source attribution is distinctly different.

Classification among a set of pre-defined sources

The task of classification among a set of pre-defined sources has frequent application to the problem of assigning the origin of a specific type of product to one of a closed set of alternatives. In this type of analysis, samples are examined and compared with a library of alternative reference samples. This is the typical laboratory support for product liability cases and enforcement cases relating to importation of goods.[2] A typical question posed to the analyst is, "From which of these possible sources (manufacturers, countries) did the sample (asbestos, lead paint, oil spill, foodstuff or defective product) come from?"

To conduct classification among a set of pre-defined sources, one must first compile "known" reference samples from each of the alternative sources in the closed set. A specific analytical protocol is then used that discriminates among the reference samples. This protocol must be based on stable, specific sample features sufficient for unambiguous discrimination. Incoming "questioned" samples are then analyzed using the same protocol and the results are compared with those from the reference set. Based on the analyses, a conclusion is made that the questioned sample is from one of the specific sources within the closed set, or that it comes from an alternative (unknown) origin. Again, this approach is very appropriate for certain types of problems, but predictive source attribution is distinctly different.

Predictive source attribution

In contrast to the comparisons with specific sources, or classification among alternative possible sources, the use of dusts for predictive source attribution works with a single sample and an open-ended set of possible sources. As noted above, the goal is to extract any intelligible "signal" that can reliably predict provenance: where items or people originated, how they have been transported, and the people, conditions and environments to which they have been exposed.

Examples of predictive source attribution from dusts are less frequent.[3] Predictive source attribution from dusts utilizes many different particle types – recognizing, analyzing and exploiting whatever particles happen to be present – and focuses on those particles providing relevant information to the source attribution questions of interest. There is a much richer signal, composed of many co-occurring particle types. With this rich, quantitative distribution of fine particles, hypotheses about the origin of the dusts can be tested, and the support for alternatives can be reliably estimated.

The exploitation of fine dusts for predictive source attribution requires a multidisciplinary approach – the goal is to recognize, identify and exploit information coming from any type of particle that is (1) present and (2) carries associated information that is useful in refining the hypothesis or solving the problem. Scientific

disciplines with consistent contributions are geology (minerals, soils), botany (pollen, plant DNA), entomology (insects, parasites), microbiology (fungi, protozoa, diatoms, foraminifera), chemistry (ingredients, drugs, explosives), industrial hygiene (work and pollution-related dusts), and forensic science (human activity traces).

We have been actively developing this capability for many years and applying it to major investigative problems including analysis and source attribution of dusts associated with counterfeits, clothing, weapons, laboratories and contraband items. Many of these investigations, at the national and international level, cannot be discussed in detail because of their ongoing or sensitive nature. The present case originated from Interpol, and approvals have been given for discussion and presentation.

The evidence resulted from a seizure of four locked steel boxes in Singapore where X-ray inspection of the boxes revealed them to be tightly packed with an estimated 1000 pounds of elephant tusks. Without opening, the locked steel boxes were tightly wrapped and shipped to the National Fish and Wildlife Forensics Laboratory in Ashland, Oregon, where we participated in the opening and sampling of evidence.

DESCRIPTION OF SAMPLES AND SAMPLE PROCESSING

A double-wrapped and tightly sealed metal shipping box was received and opened in the National Fish and Wildlife Forensics Laboratory biosafety area (Figure 1). Tusks were found tightly bundled in loosely woven fabric bags. Small particle samples (Figure 2) were collected from the fabric bags directly (falling onto clean parchment paper during bag examination), from the bottom of the shipping box, and by vacuuming of the bags using filter cassettes (see materials and methods).

Sub-samples for palynology (approximately 3 g) and non-human DNA analysis (approximately 250mg) were prepared from the vacuumed dusts by pooling small amounts from the individual cassettes. The debris recovered directly from the fabric bags and from the bottom of the box was processed for microscopical analysis and individual particle analysis. Large particles (greater than approximately 1mm) were first removed from both samples. Many of these larger particles were plant tissue, insect parts, tusk fragments and pieces of cardboard. Of the remaining, mostly fine debris, approximately one-quarter of each sample was taken by carding, resulting in a pooled sample of 1.9 grams. This sample is shown by stereomicroscopy in Figure 3. It is heterogeneous, with large quantities of mineral grains, together with smaller quantities of plant tissue and insect fragments.



Figure 1. Part of the initial opening and examination of the tusk shipment in the biosafety area of the National Fish and Wildlife Forensics Laboratory, Ashland, OR. Ken Goddard, Laboratory Director (Left) and David Stoney (Right). The tusks were tightly bundled in loosely woven fabric bags.



Figure 2. Debris recovered directly from fabric bags (top left), from the bottom of the box (top right) and by using vacuum cassettes (bottom).

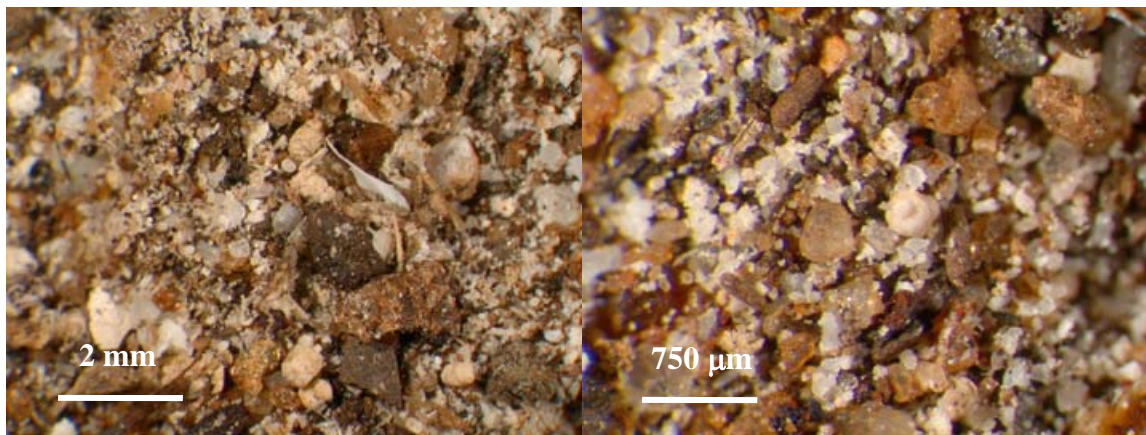


Figure 3. Overviews of the sample taken for microscopical analysis and individual particle analysis, following removal of larger particles, as shown at two different magnifications.

MATERIALS AND METHODS

Dust Recovery

Vacuum recovery of fine dusts was performed using a Staplex Model EC-1 Econometric™ Area Air Sampler, fitted with a length of Tygon® R-3603 Clear Laboratory Tubing (I.D. 1/4in/6.4mm; wall thickness 1/16in/1.6mm; O.D. 3/8in/9.5mm) and a Pall® 37mm Air Monitoring Cassette (product number 4336, 3-piece unit with 0.8 μm GN-4 Metrical® membrane and support pad). The open-faced sampling configuration was used, sweeping the cassette over the fabric while in direct contact with the fabric surface.

Particle Microscopy

Stereoscopic microscopy and photomicrography were performed using a Leica MZ16 stereomicroscope fitted with a Nikon model 995 digital camera using a 1.0X Optem coupler. Compound light microscopy (transmitted, reflected and polarized) was performed using a Zeiss Axio Imager.A1m microscope fitted with a Zeiss MRc5 digital camera using a 1.0X Zeiss coupler.

Fractionation of the Sample by Settling Velocity

Particles were fractionated by settling velocity in distilled water. The sample was added to a 15ml centrifuge tube and approximately 10 to 12 ml of distilled water was added (sufficient to allow a settling distance of 10cm). The sample was sonicated briefly and stirred. After mixing, the sample was allowed to settle in the water for 30 seconds, after which the water and portion of soil still suspended were removed from the tube using a pipette. Clean water was added to the settled sample and the procedure was repeated until there was virtually no material suspended in the water after 30 seconds of settling. The clean, settled portion was designated as the "Sand" fraction. The remaining unsettled portion was mixed and allowed to settle for 60 minutes. The portion still

suspended was removed from the tube using a pipette and was labeled, designated as the "Clay" fraction. The settled portion was labeled, designated as the "Silt" fraction.

Fractionation of Larger Particles by Sieving

The particles from the "Sand" fraction were dry sieved into four size fractions using 38 mm diameter ASTM stainless steel wire mesh sieves (Endecotts Ltd., London) of sizes 1 mm, 500 μ m and 180 μ m mesh sizes. The resulting particle size ranges of the fractions were: > 1 mm, 500 μ m - 1 mm, 180 - 500 μ m, and <180 μ m.

Fractionation of the Particles by Density Separation

The finest sieved fraction from the settled "Sand" fraction (<180 μ m) was divided into heavy and light particles by a heavy liquid density separation. The particles were placed in a clean 15 mL centrifuge tube and approximately 6.0 mL of bromoform (density = 2.89) was added. The sample was mixed and centrifuged until the partitioning of particles (floating vs. sinking) was visually complete. The bottom of the tube (containing particles with densities greater than 2.89) was then immersed in liquid nitrogen and frozen. The top portion of the bromoform, containing the light particles, was transferred to a clean centrifuge tube. Acetone was added to both tubes to decrease the density of the bromoform until all particles sank. The samples were centrifuged and the liquid was removed with a pipette. The samples were washed with acetone until all bromoform was removed from the samples. The tubes were then left uncovered on a clean bench to evaporate the remaining acetone.

Mounting of Particles for Polarized Light Microscopy (PLM)

The particle fractions isolated by density separation were prepared for polarized light microscopy (PLM) by mounting in Cargille calibrated refractive index liquids (Cargille Laboratories, Cedar Grove, NJ), using refractive index of 1.540 (n_D , 25°C, Cargille Series A) for the light particles and refractive index 1.660 (n_D , 25°C, Cargille Series B) for the heavy particles.

Identification of Sand Fraction Particles

The particles present in the fractions were characterized optically and morphologically. Identifications of minerals were made using the PLM by comparison to known samples and reference data.[4, 5]

Quantitative Estimations and Quantitative Measurements of Particle Abundance

For quantitative estimates, each particle type (such as a particular mineral) was characterized as being a major, minor or trace component of the mixture, with major defined as any particle composing greater than 10% of the sample, minor as any particle composing 1-10% of the sample, and trace as composing less than 1% of the sample. These estimates were made on a visual basis, with ambiguities addressed by verbal

modifiers, such as "low major", or "high minor", as appropriate. For quantitative determinations, number percents were determined for particle types by point counting using the ribbon method.[6]

Silt and Clay Fraction Examination by PLM

The silt and clay fractions were each suspended in water and vortexed, after which a small drop of the suspension was examined under a cover slip by PLM.

Clay Analysis by X-Ray Diffraction

A sub-sample of the re-suspended clay fraction was taken for x-ray diffraction analysis. Four different assays were sequentially performed on the sample: one on the neat clay, then again after treatment with ethylene glycol, and then again after heat treatments at two different levels. The neat clay was prepared by spotting onto a glass slide and drying in air. After x-ray diffraction, the glass slide was placed overnight in a vacuum desiccator in contact with vapor saturated with ethylene glycol. After x-ray diffraction the glass slide was heated to 400 °C in a muffle furnace for one hour. After x-ray diffraction, the slide was heated to 550 °C in a muffle furnace for one hour, followed by the final x-ray diffraction. The x-ray diffraction was performed on a PANalytical X'Pert Pro diffractometer using copper radiation, with 40 mA current and 45kV voltage, and a step size 0.033° 2-theta, both using standard conditions (4° to 64° 2-theta, 160 sec) and using a slow scan (300 sec) over the clay region (4° to 34° 2-theta) with step size 0.033° 2-theta. The resulting diffraction patterns were then compared and analyzed using the X'Pert HighScore program utilizing the International Centre for Diffraction Data (ICDD) database.

Palynology of the Silt Fraction

A sub-sample of the re-suspended silt fraction was taken for palynology. The sample was extremely difficult to process for palynology due to clumping. It was initially processed with concentrated HF (to remove silicates), followed by rinsing in concentrated HCl (to remove the resulting fluorosilicates), and dispersal in glacial acetic acid. This was followed by acetolysis (one part sulfuric acid and nine parts acetic anhydride) to remove cellulosic materials, followed by a glacial acetic acid wash. To remove atypical clumping the sample was sieved carefully through a 40µm mesh NITEX screen with subsequent preparation of two samples, one from the material larger than 40µm in size (trapped on the screen surface) and the second from the materials that were smaller than 40µm in size (having passed through the screen). Subsequent preparation consisted of washing in ethanol, dilution to 1:1 ethanol and water, staining with saffarin, addition of glycerine and allowing the ethanol to evaporate overnight. Slides were prepared and examined from both fractions, combining the results. Strictly quantitative methods of pollen counting were not performed due to high quantities of

debris. Pollen types that were identified were assessed semi-quantitatively as follows, based on observing some 250 to 300 grains:

- Abundant = dominant pollen types
- Frequently Observed = > 10 pollen grains
- Occasionally Observed = 3-10 pollen grains
- Rarely Observed = 2-3 pollen grains
- Single Grains = 1 pollen grain

Non-Human DNA Analysis

DNA from botanical particles (present as fine dusts and fragments of botanical tissue) was isolated and purified from a total of approximately 0.1 g of the sample using the Qiagen DNeasy (Valencia, CA) extraction kit. 2.5 ng to 25 ng of DNA in three separate extracts was used in PCR along with primers targeting the nuclear-encoded Internal Transcribed Spacer II (ITS2) region.[7] Primer sequences used for the Internal Transcribed Spacer II region are ITS3 (forward: GCATCGATGAAGAACGCAGC) and ITS4 (reverse; TCCTCCGCTT ATTGATATGC). PCR product cloning and sequencing was performed using the Invitrogen Topo TA Cloning Kit for Sequencing following the manufacturer's guidelines. Twenty-five resulting colonies were selected for plasmid sequencing.

Nucleotide sequences were characterized using the National Institutes of Health's online GenBank, Basic Local Alignment Search Tool (BLAST), and its associated computational tools for distance-based tree drawing.

GIS Analysis

Spatial data processing, analysis, and cartographic visualization were conducted on a Dell Precision T3400 using tools within ArcGIS ArcView 9.2 software [8] with supplemental spatial data modeling performed using DIVA-GIS 5.2 software.[9] Base map data utilized in the generation of maps were obtained from ESRI.[10]

ANALYTICAL RESULTS

Judgment of Sample Suitability for Predictive Source Attribution

From preliminary results, we concluded that the quality of this sample was very well suited to this task and to the applied analytical methods. There were many particles, varied in type, suitable for addressing the questions of interest. These included geological, ecological, and human activity signals that were expected to contribute significantly to the result.

Based on our experience with similar samples, the particles recovered in this case, and the specific questions of interest, we expected to be able to: (1) limit the possible origin of this material to a narrowly defined region or regions within a single country, (2) define options for follow on actions that will further restrict the possible areas of origin, and (3) lead to sufficiently precise areas to allow for specific evaluations, exclusions or confirmation based on comparative reference information or samples.

The foundation for this assessment was:

- analysis of the ecological and geological references available for the regions of interest
- isolation and characterization of the amounts, variety and quality of particles contributing to ecological and geological signals: minerals, pollen and spores, non-human DNA and human activity related particles

Based on this overall sample assessment of suitability for predictive source attribution, a detailed first-stage analysis of the sample was conducted.

Masses of Separated Fractions

The masses of the separated fractions, and their percentages relative to the processed sample, are given in Table 1. The sample is composed of approximately 65% sand, 29% silt, and 6% clay. The sand is primarily fine sand (<180µm).

Table 1. Masses of Sample Fractions

Fraction	Size range (µm)	Mass (g)	Mass (%)
Bulk	all	1.91	100
Sand Fraction	> 1000	0.112	6
	500 - 1000	0.135	7
	180 - 500	0.367	19
	< 180	0.632	33
	Total	1.25	65
Silt Fraction	settles in 30 sec - 60 min	0.56 ⁵	29
Clay Fraction	does not settle in 60 min	0.11 ⁵	6

⁵ The mass of the combined silt and clay fractions was taken as the bulk samples mass minus the combined mass of the sand fractions. The volumes of the silt and clay fractions after centrifuging each fraction were estimated as 0.7 mL (silt) and 0.2 mL (clay). Applying an experimentally determined correction factor of 0.7 to the clay volume (when used for mass estimates) results in 83% of the combined silt+clay mass (0.56 g) for silt, and 17% (0.11 g) for clay.

The masses of the separated heavy and light particles, from a sub-sample of the fine sand (<180µm), are given in Table 2.

Table 2. Masses of Heavy and Light Particles and Minerals

		Light (< 2.89 g/cc)		Heavy (> 2.89 g/cc)	
		Mass (g)	Mass (%)	Mass (g)	Mass (%)
Fine Sand < 180µm	All particle types	0.3312	66.44	0.1673	33.56
	Minerals (including Fe-oxides) ⁶	0.1689	50.24	0.1673	49.76
	Minerals (excluding iron oxides) ⁷	0.1510	76.78	0.0457	23.22

Abundant Particle Types in the Fine Sand Fraction (<180µm)

The two most abundant particle types present in the fine sand were aggregates of corn starch grains and iron oxides, each composing nearly 30% and together making up nearly 60% of the grains counted. It is uncertain whether the iron oxides are of geologic origin or of anthropogenic origin. Many of the mineral grains observed are iron-stained, indicating that at least a portion of the iron oxides are likely to be geologic in nature.⁸

Geological Particles in the Low Density Fine Sand Fraction

The minerals in the <180µm fraction were composed of nearly equal amounts of heavy and light minerals, with the light minerals (<2.89 g/cc) making up approximately 50% of the fraction. Overviews of the light mineral fraction by stereomicroscopy and PLM are shown in Figure 4. Point count percentages for low density (<2.89 g/cc) components of the fine size fraction are given in Table 3.

Quartz grains were the most abundant mineral present in the light mineral fraction, composing roughly 42% of the geologic material in the fraction. They are primarily well-

⁶ Adjustments based on particle percentages determined by point counting. In the light fraction non-geological particles were 51% of those counted (primarily starch aggregates, and including minor portions of organic matter such as plant tissue and charred particles).

⁷ Adjustments based on particle percentages determined by point counting. In the light fraction iron oxides accounted for 5.4% of the fraction. In the heavy fraction they accounted for 72.7% of the fraction.

⁸ The iron oxides were included in the mineralogy assessment of the sample, although the possibility that they are anthropogenic in origin, and the implications that would have on the results, are considered in the discussion and conclusions.

rounded grains, although a small number of angular quartz grains are present as well. The quartz was often iron-stained. Altered, unidentifiable mineral grains were a major component of the light fraction, making up approximately 24% of the geologic material. Feldspar minerals were also a major component, together making up about 17% of the light minerals, with a 2:1 alkali feldspar to plagioclase feldspar ratio. The feldspar grains were somewhat weathered and many were iron stained. Iron oxides were a low major component of the light mineral fraction, composing 11% of the fraction. Biotite mica was a high minor component of the fraction (7%), and there were trace amounts of lithic fragments. Figures 5 and 6 illustrate the major and minor components of the light mineral fraction.

Table 3. Point Count Percentages for Geological Particles in the Lower Density (<2.89 g/cc) Fine Sand Fraction (<180 μ m)

Particle Type	Count	Percent
Quartz	150	41.7
Alterite	85	23.6
Alkali feldspar	38	10.6
Biotite mica	38	10.6
Iron oxides	26	7.2
Plagioclase feldspar	22	6.1
Lithics	1	0.3
Total	360	100.0

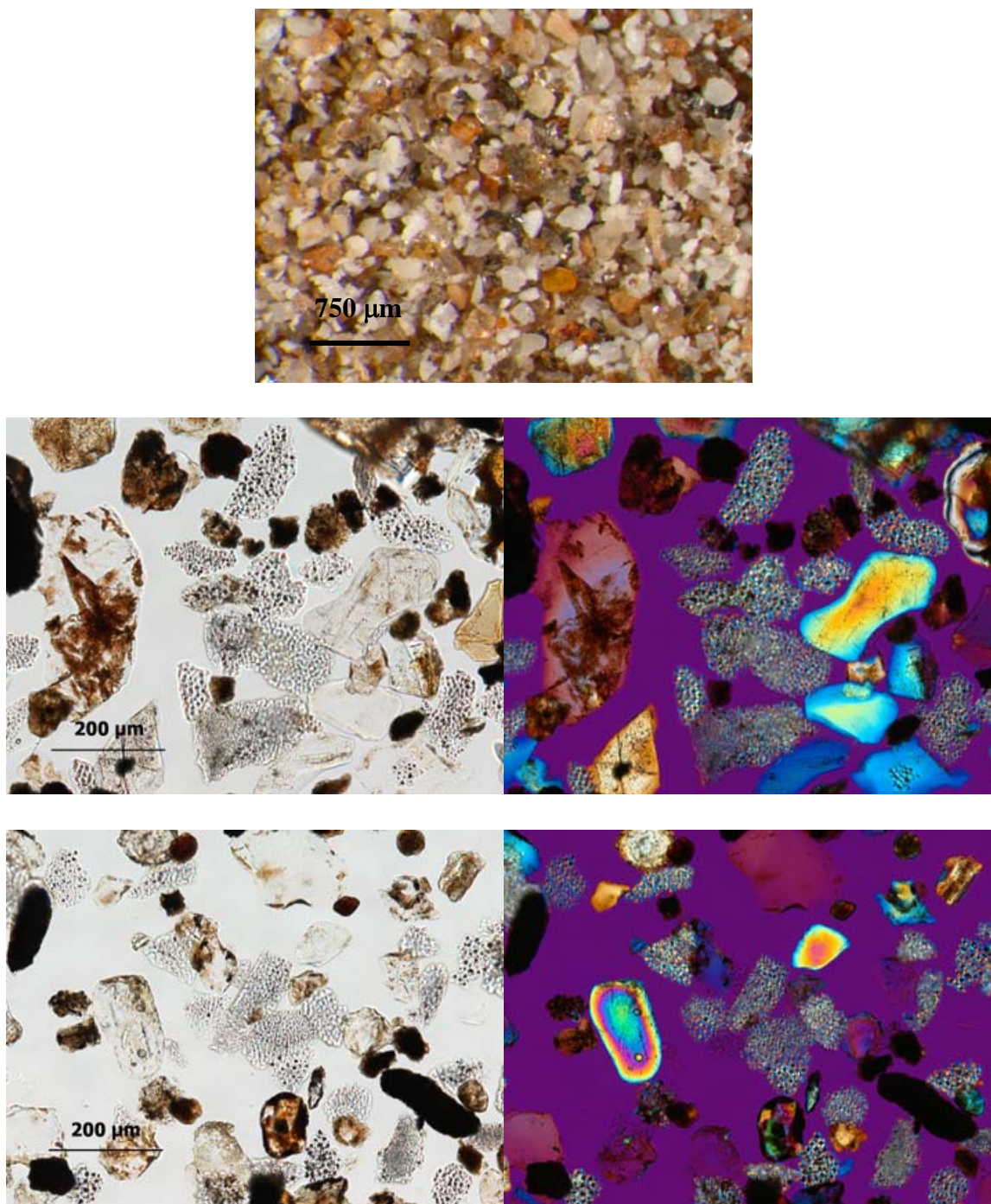


Figure 4. Top Row: Stereomicroscope overview of the light mineral fraction. Middle and Bottom Rows: Overviews of the light mineral fraction shown in plane polarized light (left), and in crossed polars with a 530 nm compensator (right). Mounting medium is 1.540.

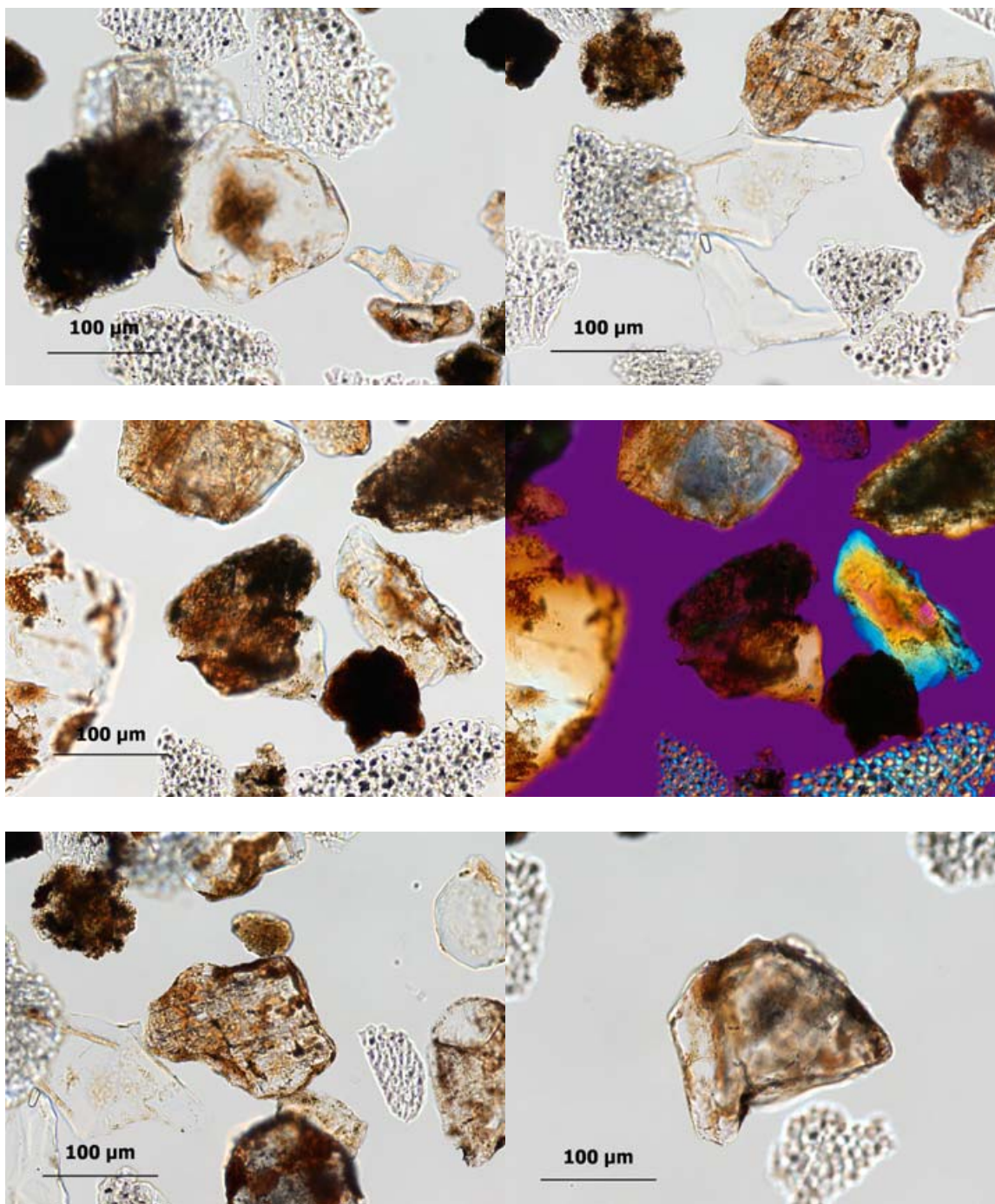


Figure 5. Top Row: A rounded quartz grain (left) and angular quartz grains (right). Second Row: Unidentified altered mineral grain in plane polarized light (left), and between crossed polars with a 530 nm compensator (right). Bottom Row: Alkali feldspar (left) and plagioclase feldspar (right). Mounting medium is 1.540.

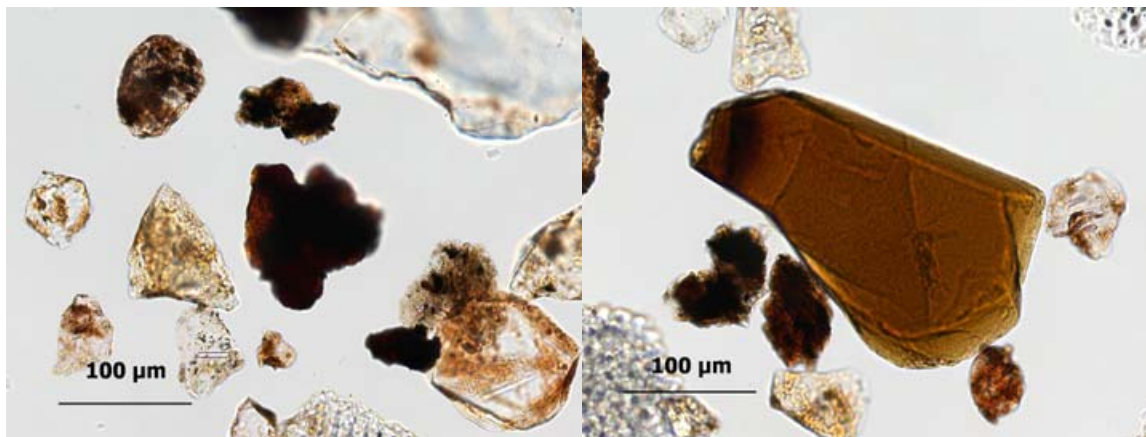


Figure 6. Iron oxide (left) and biotite mica (right). Mounting medium is 1.540.

Geological Particles in the High Density Fine Sand Fraction

The heavy minerals in the <180µm fraction comprised approximately 50% of the recovered mineral grains. An overview of the heavy mineral fraction by stereomicroscopy is shown in Figure 7 (top left). Point count percentages for high density (>2.89 g/cc) components of the fine size fraction are given in Table 4.

The heavy minerals were composed primarily of iron oxides, making up nearly 73% of the fraction. Hornblende grains were also a major component of the fraction, accounting for roughly 12% of the observed grains. Biotite mica (9%) was a high minor component. Opaque grains and muscovite mica were low minor components of the fraction. Trace components of the heavy mineral fraction were titanite, sillimanite, pyroxene, unidentifiable altered minerals, zircon, apatite, epidote, garnet, dolomite, rutile, glauconite, and an unidentified mineral. Tremolite was also observed during a survey scan following point counting. Figure 7 illustrates the major and high minor components of the heavy mineral fraction.

Particles in the Silt Fraction

There was a large amount of silt present in the recovered material (29%) and it was analyzed by PLM. The silt is dominated by corn starch grains. The minerals present consist primarily of quartz and feldspar, biotite mica, muscovite mica and iron oxides. There were smaller amounts of hornblende, opaque grains, and biological materials. Figure 8 shows an overview of the silt fraction and illustrates the primary particle components.

Table 4. Point Count Percentages for Geological Particles in the Higher Density (>2.89 g/cc) Fine Sand Fraction (<180 μ m)

Particle Type	Count	Percent
Iron oxides	812	72.7
Hornblende	129	11.5
Biotite mica	97	8.7
Opagues	29	2.6
Muscovite mica	15	1.3
Titanite	9	0.8
Sillimanite	5	0.4
Pyroxene	4	0.4
Alterite	3	0.3
Zircon	3	0.3
Apatite	3	0.3
Epidote	2	0.2
Garnet	2	0.2
Dolomite	1	0.1
Rutile	1	0.1
Glaucconite	1	0.1
(Unidentified)	1	0.1
Total	1117	100.0

Clay Fraction by Polarized Light Microscopy

By PLM the clay fraction sample showed primarily fine clay minerals and micas (Figure 9, top row). There were also minor amounts of very fine, positively elongated particles with high birefringence (Figure 9, bottom row), along with trace amounts of iron oxides and opaque particles.

Clay Fraction by X-Ray Diffraction

The XRD spectra for the neat clay fraction, and those after treatments with ethylene glycol, heating to 400 °C and heating to 550 °C are shown in Figure 10.

The peaks in the spectra are listed in Table 5, and identified crystalline phases responsible for those peaks are listed in Table 6. The XRD results indicate that the sample is composed of major illite and minor kaolinite. The presence of kaolinite was confirmed due to its behavior during heat treatment.

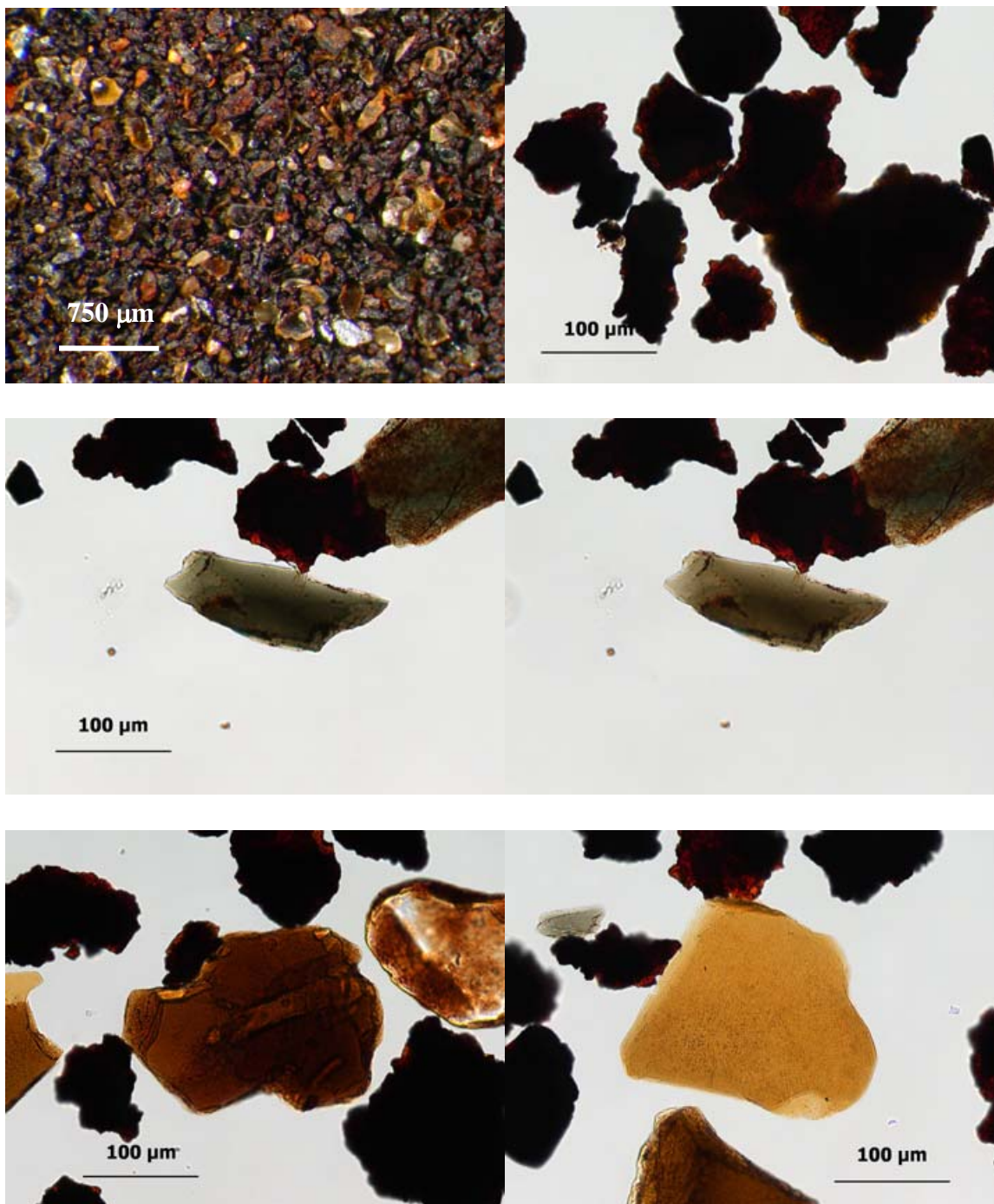


Figure 7. Top Row: Stereomicroscope overview of the heavy mineral fraction (left) and several iron oxide particles shown in plane polarized light (right). Second Row: Hornblende grain shown in plane polarized light with the polarizer oriented E-W (left) and N-S (right). Bottom Row: Biotite flakes. Mounting medium is 1.660.

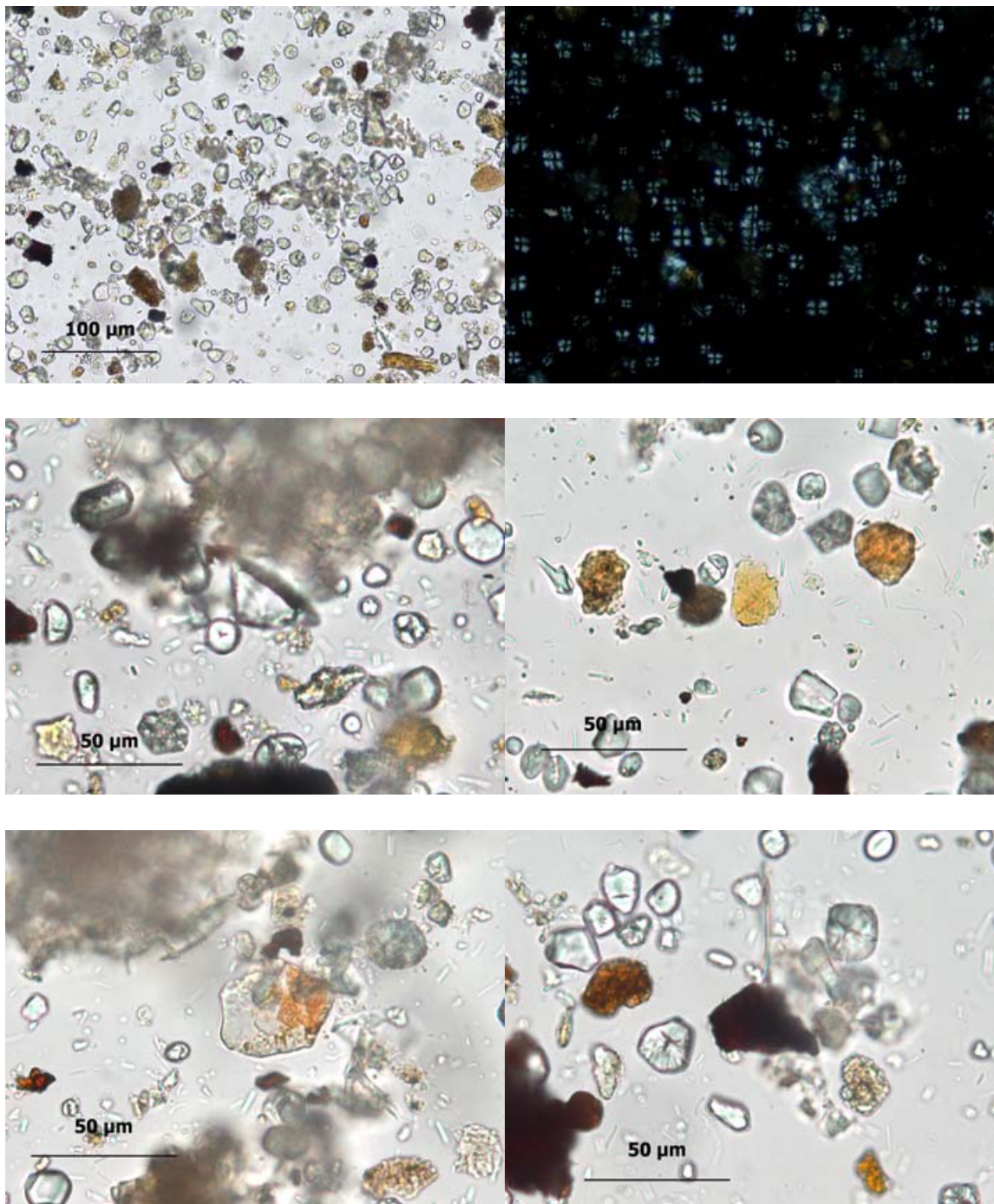


Figure 8. Top Row: Overview of the silt fraction shown in plane polarized light (left), and in between crossed polars (right). Middle Row: Quartz or feldspar grain (left) and biotite mica flake (right). Bottom Row: Muscovite mica flake (left) and iron oxide particle (right). Mounting medium is water.

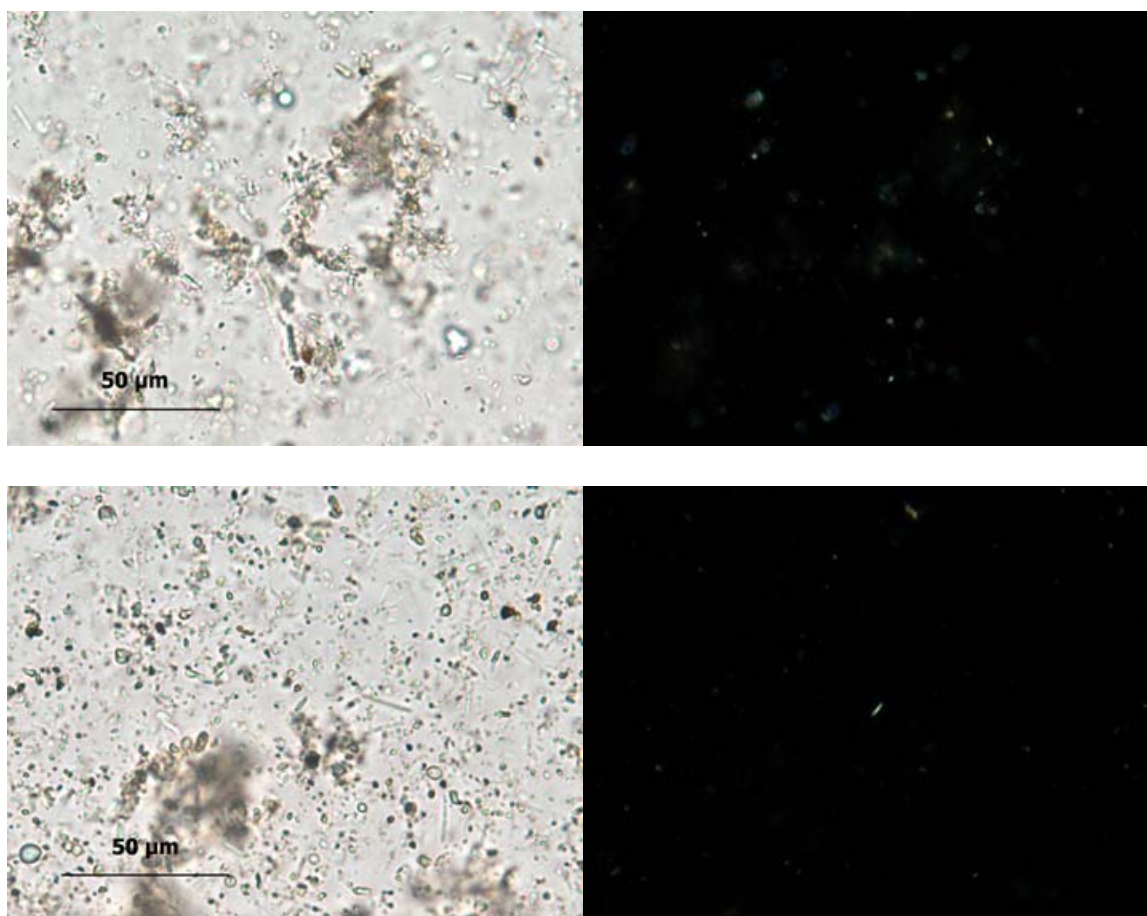


Figure 9. Top Row: Overview of the clay fraction shown in plane polarized light (top left) and in between crossed polars (top right). Bottom Row: Fine, highly birefringent particle with positive elongation shown in plane polarized light (bottom left) and in between crossed polars (bottom right). Mounting medium is water.

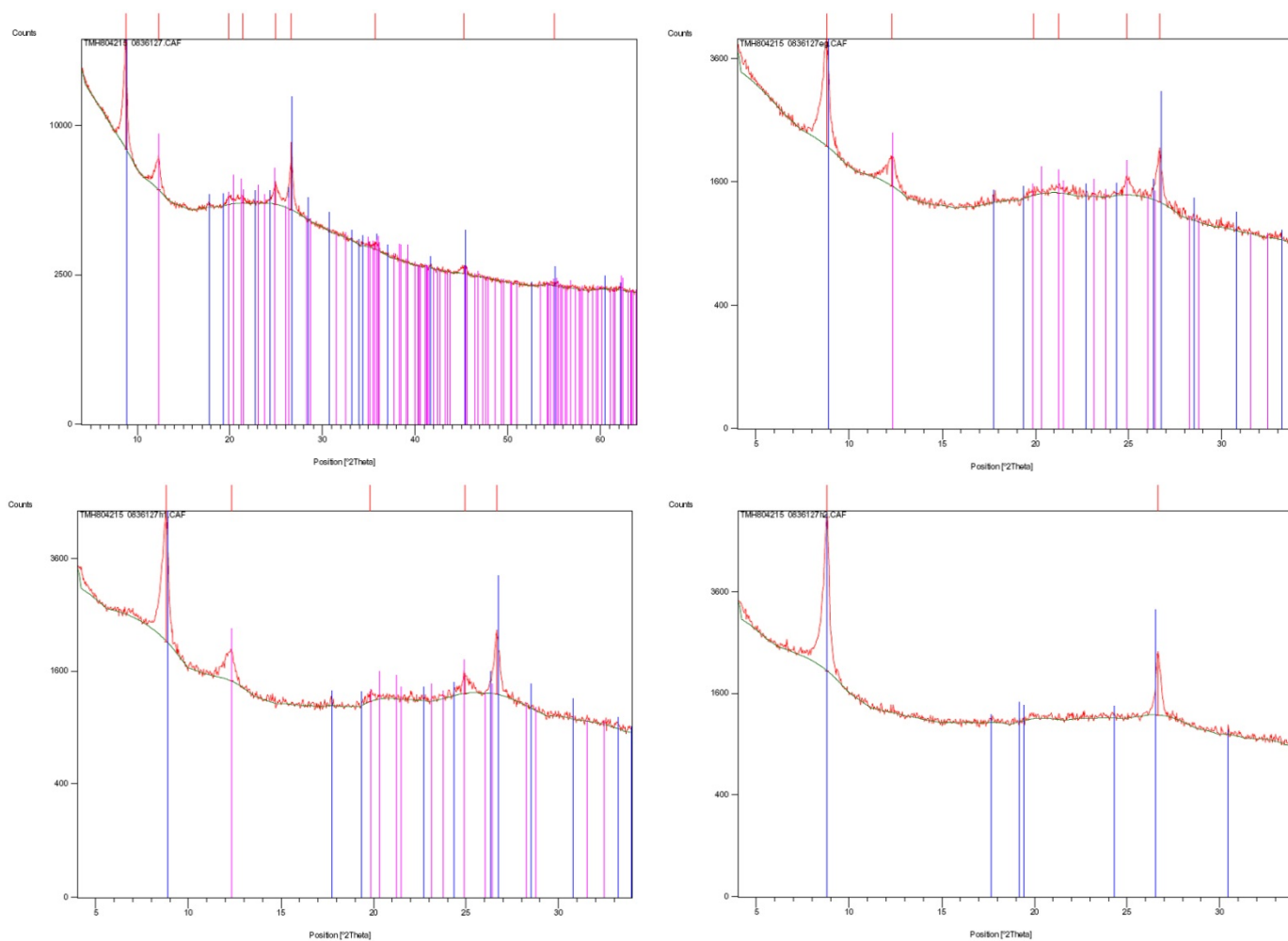


Figure 10. XRD spectra for of the clay fraction. Neat (top left), and after treatments with ethylene glycol (top right), heating to 400 °C (bottom left) and heating to 550 °C (bottom right).

Table 5. Peak Listings for Clay X-Ray Diffraction

Neat Clay

Pos. [°2Th.]	d-spacing [Å]	Area [cts*°2Th.]	Rel. Int. [%]	Matched by
8.8069	10.04093	1577.08	100.00	00-016-0344
12.3442	7.17046	247.97	23.59	01-080-0885
19.9082	4.45991	146.51	4.64	01-080-0885
21.4085	4.15064	297.85	4.05	01-080-0885
24.9229	3.57275	290.80	13.83	01-080-0885
26.6544	3.34446	476.00	45.27	00-016-0344; 01-080-0885
35.7555	2.51130	140.53	3.34	00-016-0344; 01-080-0885
45.3291	2.00069	156.97	2.49	00-016-0344; 01-080-0885
55.0171	1.66774	121.01	1.16	00-016-0344; 01-080-0885

Ethylene Glycol-Treated Clay

Pos. [°2Th.]	d-spacing [Å]	Area [cts*°2Th.]	Rel. Int. [%]	Matched by
8.8093	10.03829	482.71	100.00	00-016-0344
12.3027	7.19460	100.88	20.90	01-080-0885
19.9109	4.45932	35.06	2.42	01-080-0885
21.2458	4.18206	59.68	4.12	01-080-0885
24.9178	3.57347	59.04	12.23	01-080-0885
26.6589	3.34391	93.12	38.58	00-016-0344; 01-080-0885

400 °C Heat-Treated Clay

Pos. [°2Th.]	d-spacing [Å]	Area [cts*°2Th.]	Rel. Int. [%]	Matched by
8.8131	10.03397	497.67	100.00	00-016-0344
12.3354	7.17559	100.07	17.24	01-080-0885
19.8301	4.47731	36.64	3.68	01-080-0885
24.9272	3.57214	66.17	9.97	01-080-0885
26.6587	3.34393	182.56	36.68	00-016-0344

550 °C Heat-Treated Clay

Pos. [°2Th.]	d-spacing [Å]	Area [cts*°2Th.]	Rel. Int. [%]	Matched by
8.8150	10.03182	732.05	100.00	00-042-1437
26.6534	3.34458	200.65	27.41	00-042-1437

Table 6. Identified Crystalline Phases by X-Ray Diffraction*Neat Clay*

Visible	Ref. Code	Score	Compound Name	Scale Factor	Chemical Formula
*blue	00-016-0344	47	fluorphlogopite	0.606	$K Mg_3 (Si_3 Al) O_{10} F_2$
*pink	01-080-0885	36	Kaolinite I\ITA\RG	0.189	$Al_2 (Si_2 O_5) (O H)_4$

Ethylene Glycol-Treated Clay

Visible	Ref. Code	Score	Compound Name	Scale Factor	Chemical Formula
*blue	00-016-0344	57	fluorphlogopite	0.606	$K Mg_3 (Si_3 Al) O_{10} F_2$
*pink	01-080-0885	51	Kaolinite I\ITA\RG	0.185	$Al_2 (Si_2 O_5) (O H)_4$

400 °C Heat-Treated Clay

Visible	Ref. Code	Score	Compound Name	Scale Factor	Chemical Formula
*blue	00-016-0344	55	fluorphlogopite	0.617	$K Mg_3 (Si_3 Al) O_{10} F_2$
*pink	01-080-0885	42	Kaolinite I\ITA\RG	0.164	$Al_2 (Si_2 O_5) (O H)_4$

550 °C Heat-Treated Clay

Visible	Ref. Code	Score	Compound Name	Scale Factor	Chemical Formula
*blue	00-042-1437	62	Phlogopite- I\ITM\RG, ferroan	0.889	$K(Mg, Fe)_3 (Al, Fe) Si_3 O_{10} (OH, F)_2$

Palynology

Pollen types and their incidence observed in the examination are given in Table 7.⁹ In addition to those pollen listed in the table, there were many grains that were degraded beyond recognition and many unidentified pollen of a variety of types. The sample also contained many different taxa of fungi and many fragments of insect chitin.

Pollen types occurring abundantly, frequently or occasionally are illustrated in Figure 11. Some of the pollen types occurring more rarely in the sample are illustrated in Figure 12. Some of the many genera of fungal spores found in the sample are illustrated in Figure 13.

Dominant Pollen Types

Dominant pollen types in the sample were those of the African shrub *Adenodolichos paniculatus* (wáákén wuta, "fire bean") and the family POACEAE (grasses).

Adenodolichos paniculatu (wáákén wuta, "fire bean") is a shrub that grows best in direct sunlight. It is insect-pollinated with limited amounts of pollen. The pollen is ornate, large, and very fragile. It is not easily dispersed or carried by winds and degrades rapidly in soils.

In the POACEAE (grass family) there are hundreds of genera and thousands of species. The morphology is non-specific by light microscopy, with the principle difference among species being the pollen size. All species are wind pollinated.

Frequently Observed Pollen Types

Frequently observed pollen types on the sample were those of the species *Terminalia brownii* (hareri biiris), the genus *Rumex* (dock, sorrel), and the family COMBRETACEAE.

Terminalia brownii (hareri biiris) is a large tree that favors sandy soils and direct sunlight. The trees are commonly found in the scrublands and on the edges of savannas. It is insect-pollinated and the pollen are very small. The pollen are rarely dispersed and are only expected in soils close to the actual trees.

There are hundreds of species in the genus *Rumex* (dock, sorrel). All species need direct sunlight and they are most commonly found growing in grasslands and savanna regions. A large number of the species are wind-pollinated and disperse large quantities of pollen as far as several kilometers.

⁹ Comprehensive pollen counts (200 to 300 pollen grains per sample) were not employed for this sample because of the large amounts of debris which obscured many of the grains.

The family COMBRETACEAE are flowering plants including over 600 species of trees and shrubs. *Terminalia brownii* is in this family, but there are additional taxa represented in the sample, difficult to differentiate and which remain unidentified.

Pollen Types Observed Occasionally

Pollen types observed occasionally in the sample were those of the species *Zenkerella egregia*, the genus *Brachystegi* (miombo trees), the tribe Helianthinae (sub-family of ASTERACEAE, high spine-type) and the combined group Chen-Ams (family CHENOPODIACEAE and genus *Amaranthus*).

Zenkerella egregia is a lowland forest species of large, insect-pollinated trees. They are on the endangered species list. The pollen are only expected in soils close to the actual trees.

Brachystegi (miombo trees) are dominant and ecologically important trees occurring in large areas of open deciduous woodlands. They are insect-pollinated and the pollen are only expected in soils close to the actual trees.

The Helianthinae (ASTERACEAE, high spine type) are a large group of insect-pollinated plants, including many ornamental and weed types. They grow best in open sunlight, and are very common members of grasslands and savanna habitats.

Chen-Ams are a very large group (more than 100 genera with more than 1000 species) whose pollen are indistinguishable. Many are common weeds. All are wind-pollinated annuals that grow easily in direct sun and grow quickly in disturbed habitats. They produce vast amounts of small pollen grains that can be carried easily on wind currents.

Rarely Observed Pollen Types

Pollen types observed rarely in the sample were those of the species *Diospyros mespiliformis* (jackal berry); the genera *Citrus* (orange, lemon, etc.), *Polygonum* (knotweed), and *Typha* (monocot type cattail); the tribe Lactuceae (sub-family of ASTERACEAE, dandelion type) and the families MELIACEAE (mahogany family), MYRTACEAE (myrtle family) and RHAMNACEAE (buckthorn).

Diospyros mespiliformis (jackal berry) is a large, insect-pollinated tree, common in savannas and preferring moist soils. They produce small amounts of pollen, which are only expected in soils close to the actual trees.

Citrus (orange, lemon, etc.) is the genus that includes the commercially important species of oranges, lemons, grapefruit and limes.

Polygonum (knotweed) is a large genus of rapidly growing, mostly herbaceous plants.

There are tens of species belonging to the genus *Typha* (cattail). All of these grow in wet environments. Cattails are wind-pollinated and produce large amounts of small pollen grains that are easily dispersed by the wind.

The Lactuceae (ASTERACEAE, dandelion type) are a large group of insect-pollinated plants commonly found in fields and gardens throughout the world. They require open areas and sunlight characteristic of savanna or grassland regions.

MELIACEAE (mahogany family) is a family of about 50 genera and 550 species, mostly tropical, and including (among African species) the economically important tree species of *Carapa procera* (crabwood), *Entandrophragma cylindricum* (zapele), *Entandrophragma utile* (utile, sipo), *Guarea cedrata* (Bossé), *Khaya ivorensis* (Ivory Coast mahogany) and *Khaya senegalensis* (Senegal mahogany).

MYRTACEAE (myrtle family) is a family with over 4500 species and 130 genera which include *Myrtus* (myrtle), *Eucalyptus* (gum), and *Psidium* (guava). There are 40+ species native or introduced in Africa, and 300+ cultivated species.

RHAMNACEAE (buckthorn) is a family primarily of trees and shrubs with over 850 species and 50 genera found worldwide, but mostly in subtropical and tropical regions.

Pollen Types Observed as Single Grains

Pollen types observed as single grains were those of the species *Gilbertiodendron dewevrei* (limbali, abeum) and *Sida acuta* (common wireweed), as well as of the family CYPERACEAE (sedges).

Gilbertiodendron dewevrei (limbali, abeum) is a large African tree that grows on low, moist slopes of rivers and flooded basins. It is insect-pollinated and produces small amounts of pollen, which are expected only in soils close to the actual trees. It is commonly used for lumber, and is found in Cameroon, Central African Republic, Congo, Gabon, Ivory Coast, Liberia, Nigeria, Sierra Leone, and Zaire.

Sida acuta (common wireweed) is a shrub in the Mallow family with pantropical distribution that requires direct sunlight and grows aggressively in disturbed soils and in a wide range of environments. It is insect-pollinated and the pollen are large. The pollen are expected only in soils close to the actual trees.

Plants of the family CYPERACEAE (sedges) are most commonly found near water (marshes, bogs, edges of lakes). They are wind-pollinated, but produce low numbers of pollen which are dispersed close to the ground, so the pollen does not travel far. The pollen are fragile and degrade quickly in soils.

Table 7 Pollen Types Identified in the Sample¹⁰

Dominant Pollen Types (abundant)	Condition
<i>Adenodolichos paniculatu</i> (wáákén wuta, "fire bean")	Mix: Pristine and degraded
POACEAE (grass) with wide variety of taxa	Most degraded, few pristine
Frequently Observed Pollen Types (> 10 grains)	
<i>Terminalia brownii</i> (hareri biiris)	Pristine
<i>Rumex</i> (dock)	Most degraded, few pristine
COMBRETACEAE	Pristine
Pollen Types Observed Occasionally (3 to 10 grains)	
<i>Zenkerella egregia</i>	Pristine
<i>Brachystegi</i> (miombo trees)	Pristine
Helianthinae (ASTERACEAE, high spine type)	Pristine
Cheno-Ams	Pristine
Pollen Types Observed Rarely (2 or 3 grains)	
<i>Diospyros mespiliformis</i> (jackal berry)	Pristine
<i>Citrus</i> (orange, lemon, etc.)	Pristine
<i>Polygonum</i> (knotweed)	Pristine
<i>Typha</i> (cattail)	Pristine
Lactuceae (ASTERACEAE, dandelion type)	Pristine
MELIACEAE (mahogany family)	Pristine
MYRTACEAE (myrtle family)	Degraded
RHAMNACEAE (buckthorn)	Pristine
Pollen Types Observed as Single Grains	
<i>Gilbertiodendron dewevrei</i> (limbali, abeum)	Degraded
<i>Sida acuta</i> (common wireweed)	Pristine
CYPERACEAE (sedges)	Pristine

¹⁰ Among 250 to 300 observed grains, Abundant = dominant pollen types, Frequently observed = > 10 grains, Occasionally observed = 3-10 grains, Rarely observed = 2-3 grains.

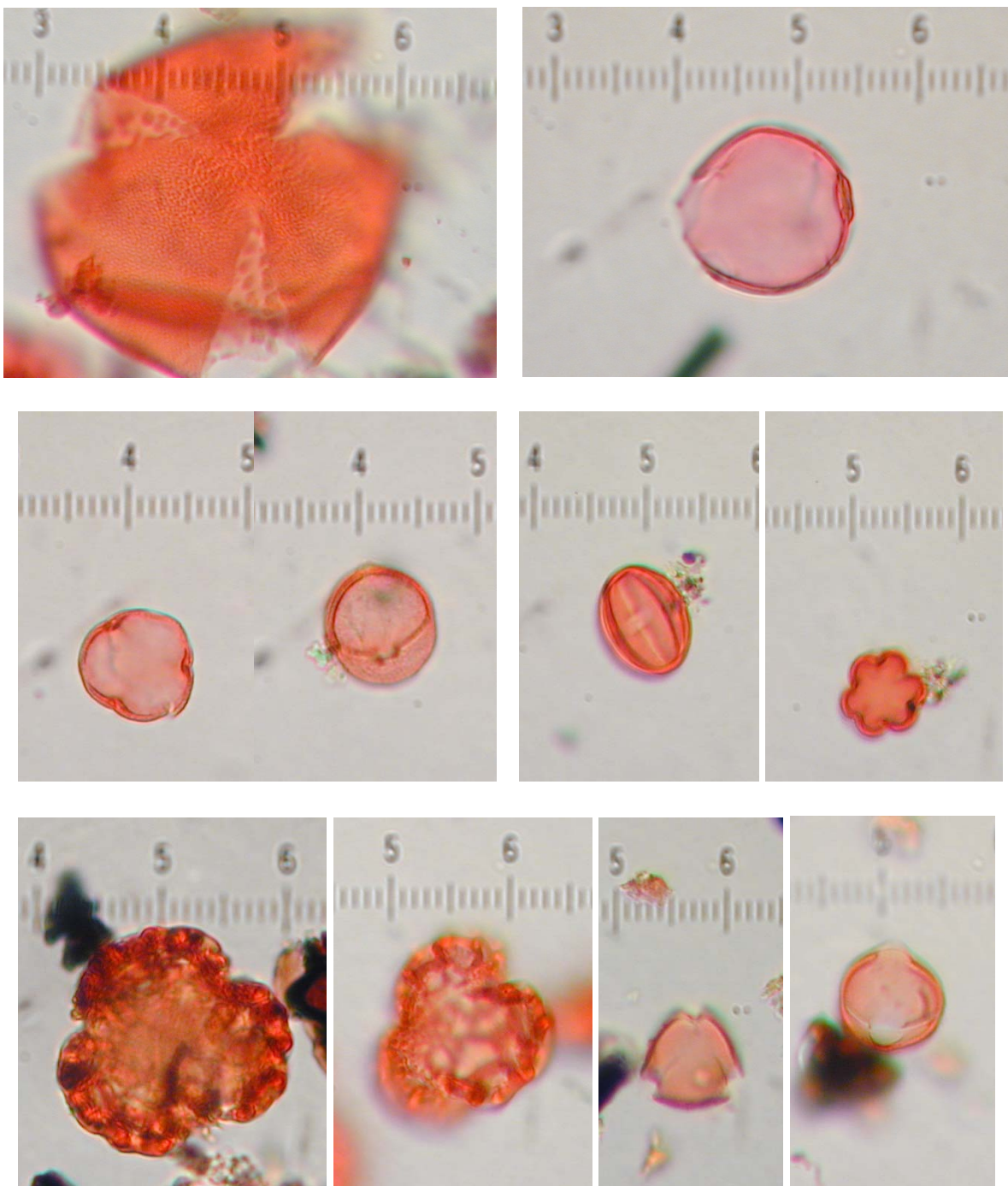


Figure 12. Some of the key pollen types in the sample. Top Row: Abundant, dominant pollen types: *Adenodolichos paniculatu* (left), and POACEAE (grass, right). Middle Row: Frequently observed pollen types: *Rumex* (two views, left) and *Terminalia brownie* (two views, right). Bottom Row: Occasionally observed pollen types: *Brachystegi* (two views, left) and *Zenkerella egregia* (two views, right). The distance between the smallest units on the scale is 2.5 μ m.

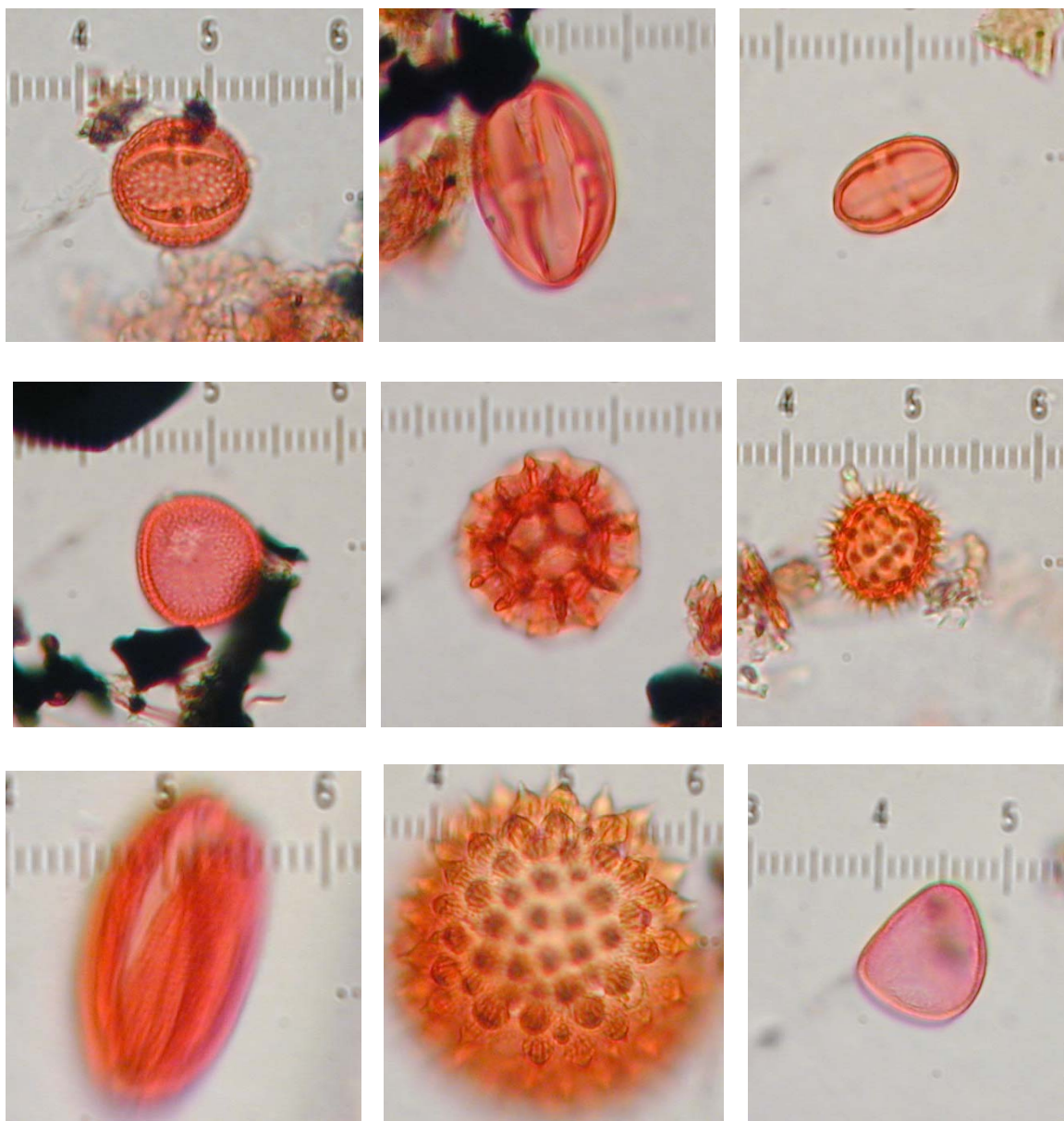


Figure 13. Some of the pollen types found in small numbers in the sample. Top Row: *Citrus*, *Diospyros mespiliformis*, and *Polygonium*. Middle Row: *Typha*, ASTERACEA (*Lactuceae* type), and ASTERACEA (*Helianthinae* type); Bottom Row: *Gilbertiodendron dewevri*, *Sida acuta*, CYPERACEAE. The distance between the smallest units on the scale is 2.5 μ m.



Figure 14. Some of the many genera of fungal spores found in the sample. The distance between the smallest units on the scale is $2.5\mu\text{m}$.

Non-Human DNA

Table 8 shows the taxa identified by their DNA. Six plant taxa were identified along with three fungal taxa.

Botanical DNA

Colophospermum mopane (mopane tree) is a characteristic tree found in Africa that grows in hot, dry, low-lying areas.

Flueggea (bushweeds) is a genus of some 50+ species. The DNA recovered from this sample had over 50% of the data sequences of this type, which is most closely related to (but distinct from) available reference DNA of *Flueggea virosa* (Chinese waterberry) and *Flueggea leucopyrus*. Bushweeds are distributed in Eastern Hemisphere tropical zones.

Bauhinia (orchid tree) is a genus of 500+ species distributed in the tropics and warm temperate climates. Many species are grown as ornamentals.

The *Triticum* (wheat genus) plant DNA is identified to genus level and could be from domestic wheat or wild varieties. Similarly, the *Zea* (corn genus) plant DNA is also identified to genus level and could be from domestic corn or wild varieties.

The FABACEAE (legume family) is very large with 700+ genera and nearly 20,000 species. The plant DNA present in the sample is most closely related to (but distinct from) available reference DNA of the genus *Podalyria* and *Calpurnia*. Both are shrubs or small trees found in southern Africa.

Fungal DNA

Aspergillus penicilloides is a common aerobic, filamentous mold. *Eurotium amstelodami* is closely related to *Aspergillus* species, as its (distinctly separate) sexually reproductive stage. The *Malassezia* fungal DNA is identified to the genus level. It is a type of yeast, naturally found on the skin surfaces of many animals (including man).

Table 8. Taxa Identified by DNA Sequence Analysis and Molecular Systematics

Plants

Colophospermum mopane (mopane tree)*Flueggea* (bushweed)*Bauhinia* (orchid tree)*Triticum* (wheat genus)*Zea* (corn genus)FABACEAE close to genus *Podalyria* or *Calpurnia*

Fungi

*Aspergillus penicilloides**Eurotium amstelodami**Malassezia***ANALYTICAL SUMMARY AND INTERPRETATIONS***Overview*

There was a strong signal of naturally occurring minerals, containing a wide variety that is well distributed by size into sand, silt and clay (enabling extensive analysis of each). There was also a very wide variety of pollen and spore types present, contributing to the signal through their individual identifications, relative quantities and condition, co-occurrences and correlations. Additional signals were identified using botanical DNA.

Geological Environment

The minerals in the sample are composed of both light and dark grains, with small quantities of plant matter and insect fragments. The grains are fairly well sorted, with most of the material being fine sand and silt, primarily in the < 180µm size range. Excluding starch and other non-geologic material, the fine sand is composed primarily of iron oxides, making up roughly 42% of the fine sand. Quartz was the next most abundant component, making up 21% of the sample and occurring primarily as rounded, iron-stained grains. Altered, unidentifiable grains were a low major component (12%); biotite (8%) and feldspar (8%) were high minor components. The feldspar was almost two-thirds alkali feldspar and one-third plagioclase, primarily occurring as iron-stained altered grains. Hornblende (6%) and opaque minerals (1%) were minor components of the sand, and there were trace amounts of plant opal, lithic fragments, muscovite mica, titanite, sillimanite, pyroxene, zircon, apatite, epidote, garnet, dolomite, rutile, glauconite, tourmaline, tremolite, and two unidentified minerals. The silt fraction contained generally similar minerals as the fine sand fraction. There was a significant amount of clay in the sample, dominated by illite along with minor kaolinite.

Excluding iron oxides (a major portion of which is likely anthropogenic), the fine sand is dominated by quartz grains (36%) and highly altered, unidentifiable minerals (20%). Feldspar minerals and biotite each make up 14% of the fine sand excluding iron oxides, and hornblende is 10% of this fraction. Opaque minerals and muscovite mica are low minor components, with trace amounts of plant opal, lithic fragments, titanite, sillimanite, pyroxene, zircon, apatite, epidote, garnet, dolomite, rutile, glauconite, tourmaline, tremolite, and two unidentified minerals.

The majority of the sediment has a composition consistent with an ironstone or iron-rich sandstone (if a major portion of the iron oxides are geologic in origin) or a feldspathic sandstone (if a major portion of the iron oxides are anthropogenic). There is likely an intermediate or mafic rock that contributed to the sediment, as indicated by the relatively large amounts of biotite and hornblende. The rounded nature of the quartz and weathered nature of the feldspar minerals indicates that this is likely from fairly mature sediment, supported by the significant amount of kaolinite clay. The virtual absence of carbonates (a single dolomite grain in the heavy fraction was the only carbonate observed) indicates that there is no limestone in the vicinity. The sample contained a relatively large amount of mineral grains significantly larger than 60 μ m, and there were no characteristic volcanic minerals or morphologies observed. This indicates that there are unlikely to be volcanic rocks contributing to the sediment.

Overall, the geological analysis indicates the minerals originated from ironstone or sandstone, or from a sedimentary deposit of aeolian or fluvial nature.

Ecological Environment

Based on the pollen, fungal spores and DNA there is strong support for a tropical region.

- Pollen from insect-pollinated plants are dominant. Most tropical plants are insect pollinated.
- A bimodal pollen size distribution was observed. This is typical for tropical regions, and atypical for temperate regions. In tropical regions (and in this sample), most of the pollen are either small (5 to 25 μ m) or large (50 to 100 μ m). In temperate regions, on the other hand, the vast majority of pollen types range in size between 25 and 45 μ m in diameter.
- Many fungi are present, in high diversity, along with many pollen grains that were degraded beyond recognition. This is typical for warm and humid habitats in tropical regions, where microbial activity and chemical oxidation are high.

The fungal spores are more resistant to oxidation, and much of the pollen become highly degraded.

- Botanical taxa identified by DNA are characteristic of tropical environments. This includes *Flueggea* (bushweeds), *Bauhinia* (orchid tree), *Podalyria/Calpurnia*, and *Colophospermum mopane* (mopane tree).

Within the tropical region, there is strong support for a dominant grassland or savanna habitat.

- The abundance and diversity of grasses indicate grasslands or savannas.
- All of the pollen types that were dominant, frequently observed, or occasionally observed come from plants that are typical of savanna and/or open brushland environments. For the most part, these plants are annuals, quick growing, and require open sunlight.

Near the specific site there is a dominant presence of the *Adenodolichos paniculatus* shrub (wáákén wuta, "fire bean") and *Flueggea* (bushweeds).

Within the dominant grassland environment, or closely nearby, there is strong support for scrubland and trees.

- The following trees and shrubs were present: *Terminalia brownii* (hareri biiris), *Brachystegi* (miombo), *Colophospermum mopane* (mopane) , *Bauhinia* (orchid tree) and *Podalyria / Calpurnia*.
- Pollen (occurring in small numbers) are present from an assortment of additional trees and shrubs:
 - *Diospyros mespiliformis* (jackal berry)
 - *Citrus* (orange, lemon, etc.)
 - *Polygonum* (knotweed)
 - MELIACEAE (mahogany family)
 - MYRTACEAE (myrtle family)
 - RHAMNACEAE (buckthorn family)
 - *Gilbertiodendron dewevrei* (limbali, abeum)

There is support for a nearby wetter area. Close by (within an easy wind-blown distance) are *Typha* (cattails), and CYPERACEAE (sedges).¹¹

¹¹ *Although sedges are only indicated by a single pollen grain, this grain is in excellent condition and pollen of this type are (1) produced in low numbers, (2) dispersed close to the ground, and (3) quickly degraded in soil.*

GEOGRAPHICAL INFERENCES

A First Stage Source Attribution Estimate¹² was made based on four primary geographical inferences:

- an initial environmental estimate (based primarily on botanical findings)
- an initial soil estimate (based primarily on mineral findings)
- a taxonomic viability estimate for *Diospyros mespiliformis*
- a taxonomic occurrence estimate for *Colophospermum mopane*

A combined intersection of these estimates resulted in the overall First Stage Source Attribution Estimate.

An Initial Environmental Estimate

A review was conducted of ecoregion profiles [11,12] and their corresponding reports as described in *Terrestrial Ecoregions of Africa and Madagascar: A Conservation Assessment* [13] to assess their correspondence with the potential source environment as inferred from the initial analysis of the small particle traces from the sample. The geographical distribution of these reference data is mapped in Figure 15, using the WWF Terrestrial Ecoregions dataset.[14]

Based on the degree of correspondence with the initial fine particle analysis, twenty-six ecoregions were classified as Excluded and 15 were found to have Poor Fit correspondence (Table 9). This assessment was based primarily on botanical signals (pollen and plant DNA) and to a lesser extent on mineralogical signals (e.g. soil). The remaining 65 ecoregions within Africa contain at least one botanical or ecological feature that could contribute to the signals obtained from the sample. This initial environmental assessment was mapped using GIS by reclassifying the WWF Terrestrial Ecoregions dataset into three classes: Possible, Poor Fit, and Excluded as a potential source of the observed environmental signals. The result is shown Figure 16, where the dark gray shows Excluded regions, the lighter gray, Poor Fit regions, and the white showing possible remaining regions.

¹² See discussion in the following section, "Next Steps."

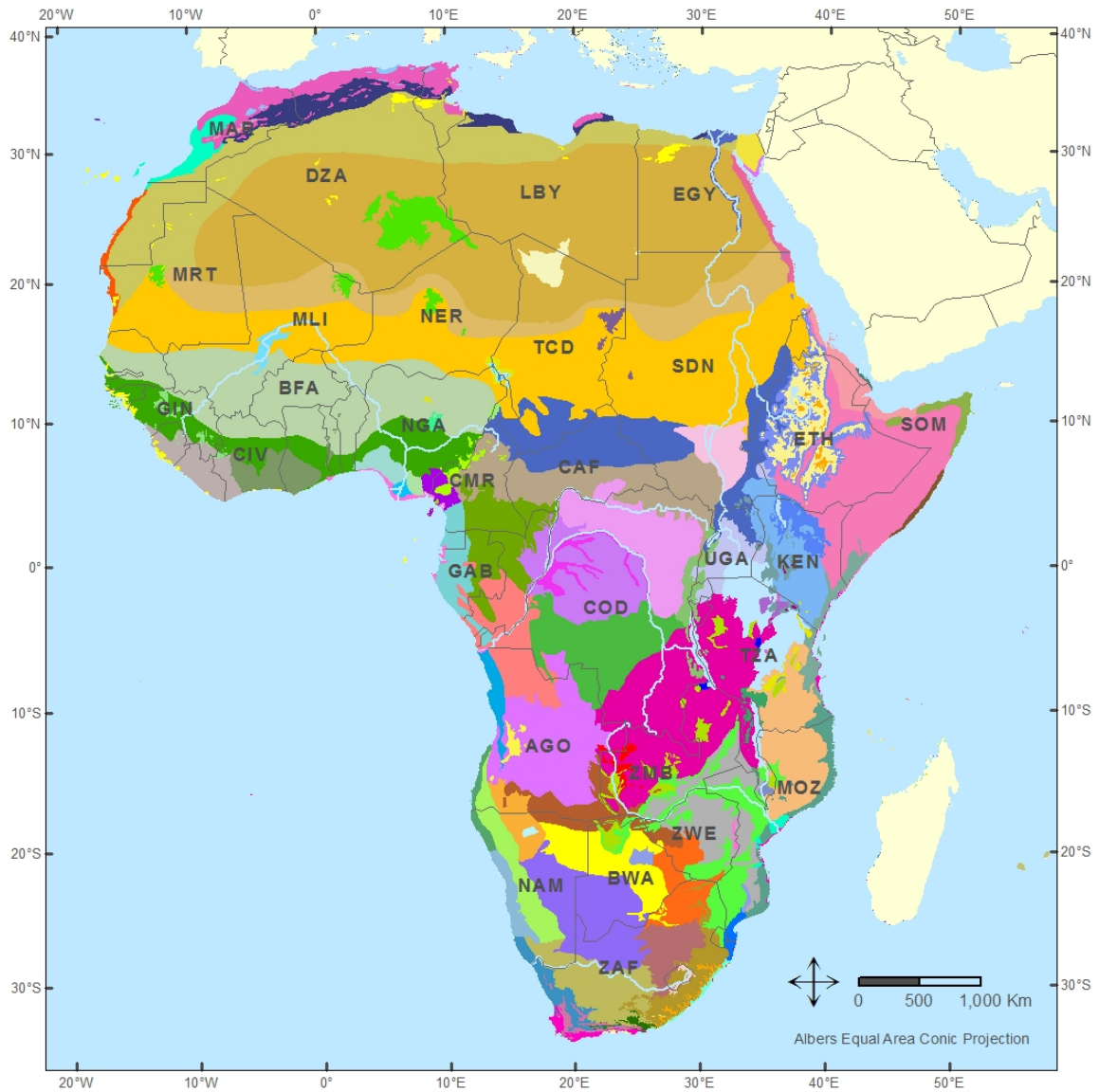


Figure 15. Map illustrating the WWF Terrestrial Ecoregions dataset within continental Africa. There are a total of 106 ecoregions within this area.

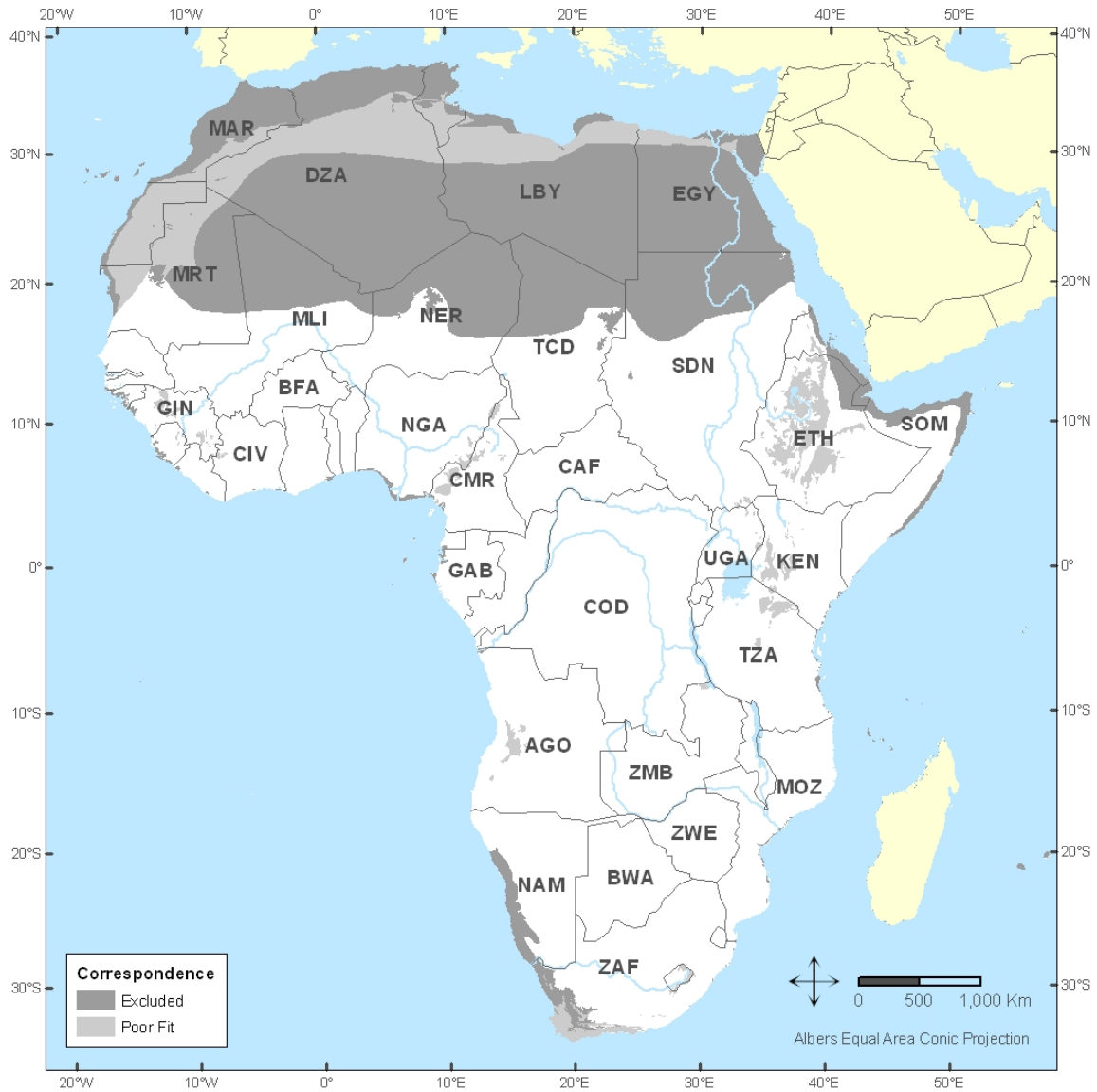


Figure 16. An initial environmental assessment for the African continent. Excluded areas are shown in dark gray. Highly unlikely Poor Fit areas are shown in light gray.

Table 9. Summary of Ecoregions Classified as Excluded or with Poor Fit Correspondence with Observed Environmental Signals

Eco-Code	Realm	Biome	Ecoregion	Class
AT0103	Afrotropic	Tropical and Subtropical Moist Broadleaf Forests	Cameroonian Highlands forests	Poor Fit
AT0108	Afrotropic	Tropical and Subtropical Moist Broadleaf Forests	East African montane forests	Poor Fit
AT0114	Afrotropic	Tropical and Subtropical Moist Broadleaf Forests	Guinean montane forests	Poor Fit
AT0115	Afrotropic	Tropical and Subtropical Moist Broadleaf Forests	Knysna–Amatole montane forests	Poor Fit
AT0121	Afrotropic	Tropical and Subtropical Moist Broadleaf Forests	Mount Cameroon and Bioko montane forests	Poor Fit
AT0708	Afrotropic	Tropical and Subtropical Grasslands, Savannas, and Shrublands	Itigi–Sumbu thicket	Poor Fit
AT0710	Afrotropic	Tropical and Subtropical Grasslands, Savannas, and Shrublands	Mandara Plateau mosaic	Poor Fit
AT0714	Afrotropic	Tropical and Subtropical Grasslands, Savannas, and Shrublands	Serengeti volcanic grasslands	Poor Fit
AT1001	Afrotropic	Montane Grasslands and Shrublands	Angolan montane forest–grassland mosaic	Poor Fit
AT1003	Afrotropic	Montane Grasslands and Shrublands	Drakensberg alti–montane grasslands and woodlands	Poor Fit
AT1007	Afrotropic	Montane Grasslands and Shrublands	Ethiopian montane grasslands and woodlands	Poor Fit
AT1008	Afrotropic	Montane Grasslands and Shrublands	Ethiopian montane moorlands	Poor Fit
AT1202	Afrotropic	Mediterranean Forests, Woodlands, and Shrublands	Lowland fynbos and renosterveld	Poor Fit
AT1203	Afrotropic	Mediterranean Forests, Woodlands, and Shrublands	Montane fynbos and renosterveld	Poor Fit

Eco-Code	Realm	Biome	Ecoregion	Class
AT1303	Afrotropic	Deserts and Xeric Shrublands	East Saharan montane xeric woodlands	Excluded
AT1304	Afrotropic	Deserts and Xeric Shrublands	Eritrean coastal desert	Excluded
AT1305	Afrotropic	Deserts and Xeric Shrublands	Ethiopian xeric grasslands and shrublands	Excluded
AT1307	Afrotropic	Deserts and Xeric Shrublands	Hobyos grasslands and shrublands	Excluded
AT1315	Afrotropic	Deserts and Xeric Shrublands	Namib desert	Excluded
AT1317	Palaearctic	Deserts and Xeric Shrublands	Red Sea coastal desert	Excluded
AT1319	Afrotropic	Deserts and Xeric Shrublands	Somali montane xeric woodlands	Excluded
AT1322	Afrotropic	Deserts and Xeric Shrublands	Succulent Karoo	Excluded
AT1401	Afrotropic	Mangroves	Central African mangroves	Excluded
AT1402	Afrotropic	Mangroves	East African mangroves	Excluded
AT1403	Afrotropic	Mangroves	Guinean mangroves	Excluded
AT1405	Afrotropic	Mangroves	Southern Africa mangroves	Excluded
PA0513	Palaearctic	Temperate Conifer Forests	Mediterranean conifer and mixed forests	Excluded
PA0904	Palaearctic	Flooded Grasslands and Savannas	Nile Delta flooded savanna	Excluded
PA0905	Palaearctic	Flooded Grasslands and Savannas	Saharan halophytics	Excluded
PA1010	Palaearctic	Montane Grasslands and Shrublands	Mediterranean High Atlas juniper steppe	Excluded
PA1212	Palaearctic	Mediterranean Forests, Woodlands, and Shrublands	Mediterranean acacia-argania dry woodlands and succulent thickets	Excluded
PA1213	Palaearctic	Mediterranean Forests, Woodlands, and Shrublands	Mediterranean dry woodlands and steppe	Excluded
PA1214	Palaearctic	Mediterranean Forests, Woodlands, and Shrublands	Mediterranean woodlands and forests	Excluded

Eco-Code	Realm	Biome	Ecoregion	Class
PA1303	Palaearctic	Deserts and Xeric Shrublands	Arabian Desert and East Sahero-Arabian xeric shrublands	Excluded
PA1304	Palaearctic	Deserts and Xeric Shrublands	Atlantic coastal desert	Excluded
PA1321	Palaearctic	Deserts and Xeric Shrublands	North Saharan steppe and woodlands	Poor Fit
PA1325	Palaearctic	Deserts and Xeric Shrublands	Red Sea Nubo-Sindian tropical desert and semi-desert	Excluded
PA1327	Palaearctic	Deserts and Xeric Shrublands	Sahara desert	Excluded
PA1329	Palaearctic	Deserts and Xeric Shrublands	South Saharan steppe and woodlands	Excluded
PA1331	Palaearctic	Deserts and Xeric Shrublands	Tibesti-Jebel Uweinat montane xeric woodlands	Excluded
PA1332	Palaearctic	Deserts and Xeric Shrublands	West Saharan montane xeric woodlands	Excluded

An Initial Soil Estimate

A review was conducted of dominant soil types as defined in the UN-FAO Digital Soil Map of the World[15] to assess their correspondence with the potential source location as inferred from the initial analysis of the small particle traces from the sample. The geographical distribution of these reference data within continental Africa is mapped in Figure 17.

Based on the degree of correspondence of soil descriptions with the initial fine particle analysis, 20 dominant soil types were excluded as possible source locations, and seven were classified as having poor fit as a potential source location (Table 10). The remaining 60 dominant soil type remained as possible source locations. This initial soil correspondence assessment was mapped using GIS by reclassifying the dominant soil types of the Digital Soil Map of the World dataset as Possible, Poor Fit, or Excluded potential source locations. The result is shown Figure 18, where the dark gray shows Excluded regions, the lighter gray, Poor Fit regions, and the white showing possible remaining regions.

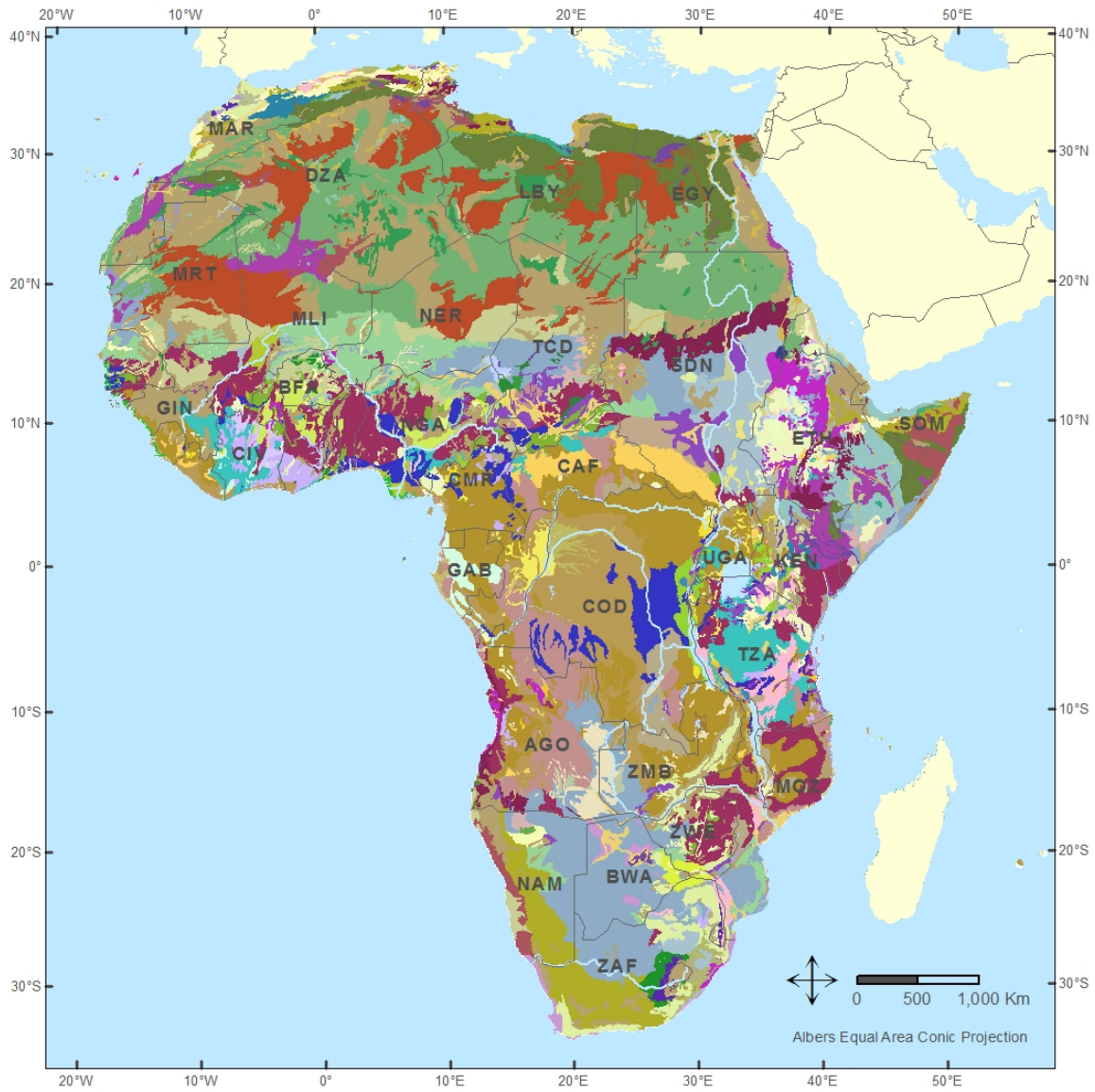


Figure 17. Map illustrating the UN-FAO Digital Soil Map of the World dataset within continental Africa. There are a total of 87 dominant soil types within this area.

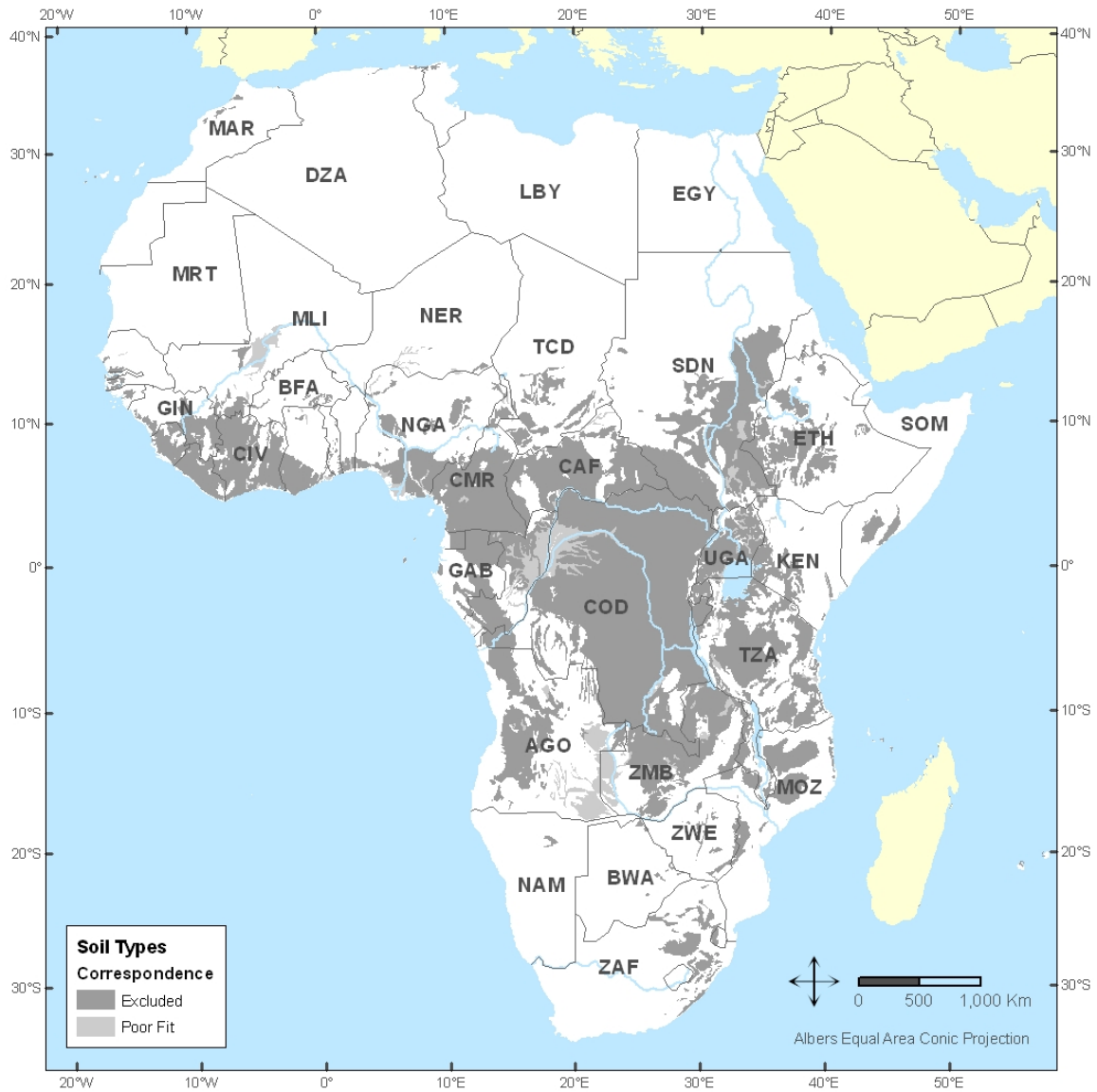


Figure 18. An initial soil assessment for the African continent. Excluded areas are shown in dark gray. Highly unlikely Poor Fit areas are shown in light gray.

Table 10. Summary of Soil Types Classified as having Poor Fit Correspondence with Geological Signals or Excluded as a Potential Source Location

Soil Type	Class
Af: Ferric Acrisols	Excluded
Ag: Gleyic Acrisols	Excluded
Ah: Humic Acrisols	Excluded
Ao: Orthic Acrisols	Excluded
Ap: Plinthic Acrisols	Excluded
Fa: Acric Ferralsols	Excluded
Fh: Humic Ferralsols	Excluded
Fo: Orthic Ferralsols	Excluded
Fp: Plinthic Ferralsols	Excluded
Fr: Rhodic Ferralsols	Excluded
Fx: Xanthic Ferralsols	Excluded
Gc: Calcaric Gleysols	Poor Fit
Gd: Dystric Gleysols	Poor Fit
Ge: Eutric Gleysols	Poor Fit
Gh: Humic Gleysols	Poor Fit
Gm: Mollic Gleysols	Poor Fit
Gp: Plinthic Gleysols	Poor Fit
Gx: Gelic Gleysols	Poor Fit
Nd: Dystric Nitosols	Excluded
Ne: Eutric Nitosols	Excluded
Nh: Humic Nitosols	Excluded
Th: Humic Andosols	Excluded
Tm: Mollic Andosols	Excluded
To: Ochric Andosols	Excluded
Tv: Vitric Andosols	Excluded
Vc: Chromic Vertisols	Excluded
Vp: Pellic Vertisols	Excluded

A Taxonomic Viability Estimate for Diospyros mespiliformis

Pollen present in the sample showed the proximity of the African ebony or jackal berry tree (*Diospyros mespiliformis*). This species is a medium to large sized tree that is widespread in tropical regions of Africa. It is most commonly found in savannas and savanna woodlands at elevations below 1,300 m, and is absent from the rain forests of the Guinea Congolian Region except locally along their northern fringes. A taxonomic viability estimate was made based on climate suitability using the EcoCrop modeling approach and DIVA-GIS software.[16] This climate suitability model uses long-term monthly temperature and precipitation data from the WorldClim database [17] to predict the adaptation of a specific plant over geographic areas based on the precipitation, temperature, and growing season thresholds. These climate suitability parameters for *Diospyros mespiliformis* were taken from the EcoCrop online database.[18]

The EcoCrop model generated six categories for the potential growth of *Diospyros mespiliformis*: Excellent, Very Suitable, Suitable, Marginal, Very Marginal and Unsuitable. Figure 19 shows the areas ranging from Excellent to Suitable as green, and those from Marginal to Very Marginal as yellow. The white areas are Unsuitable for the potential growth of *Diospyros mespiliformis*.

A Taxonomic Occurrence Estimate for Colophospermum mopane

The mopane tree, *Colophospermum mopane* was detected in the sample by DNA analysis. This species is a conspicuous and well-recognized one, which occurs as either a shrub or tree depending on local conditions. The range of the genus *Colophospermum* is described in a number of flora references [19–25]. It is endemic to the Zambebian floristic region of southern Africa, which encompasses approximately 3,770,000 sq km. There is a recorded distribution within parts of Angola, Botswana, Malawi, Mozambique, Namibia, South Africa, Zambia, and Zimbabwe. There are no significant records of this species being cultivated outside of its native distribution.

African ecoregion profiles [11–13] were reviewed for the recorded presence of *Colophospermum mopane* as a dominant, common, or noteworthy vegetation type. Ecoregions without a recorded presence of mopane were assessed to determine whether they could support this species in ecotone or transitional environments, such as in proximity to borders with ecoregions having a recorded presence of mopane. Nine ecoregions were found to have a recorded presence of mopane, and seven ecoregions were found to contain transitional areas and / or ecological features that could support the presence of mopane (Table 11). This taxonomic occurrence assessment was mapped using GIS (Figure 20) by reclassifying the WWF Terrestrial Ecoregions dataset [14] according to the recorded presence, possible presence, or no recorded presence of mopane in the respective ecoregions of Africa.

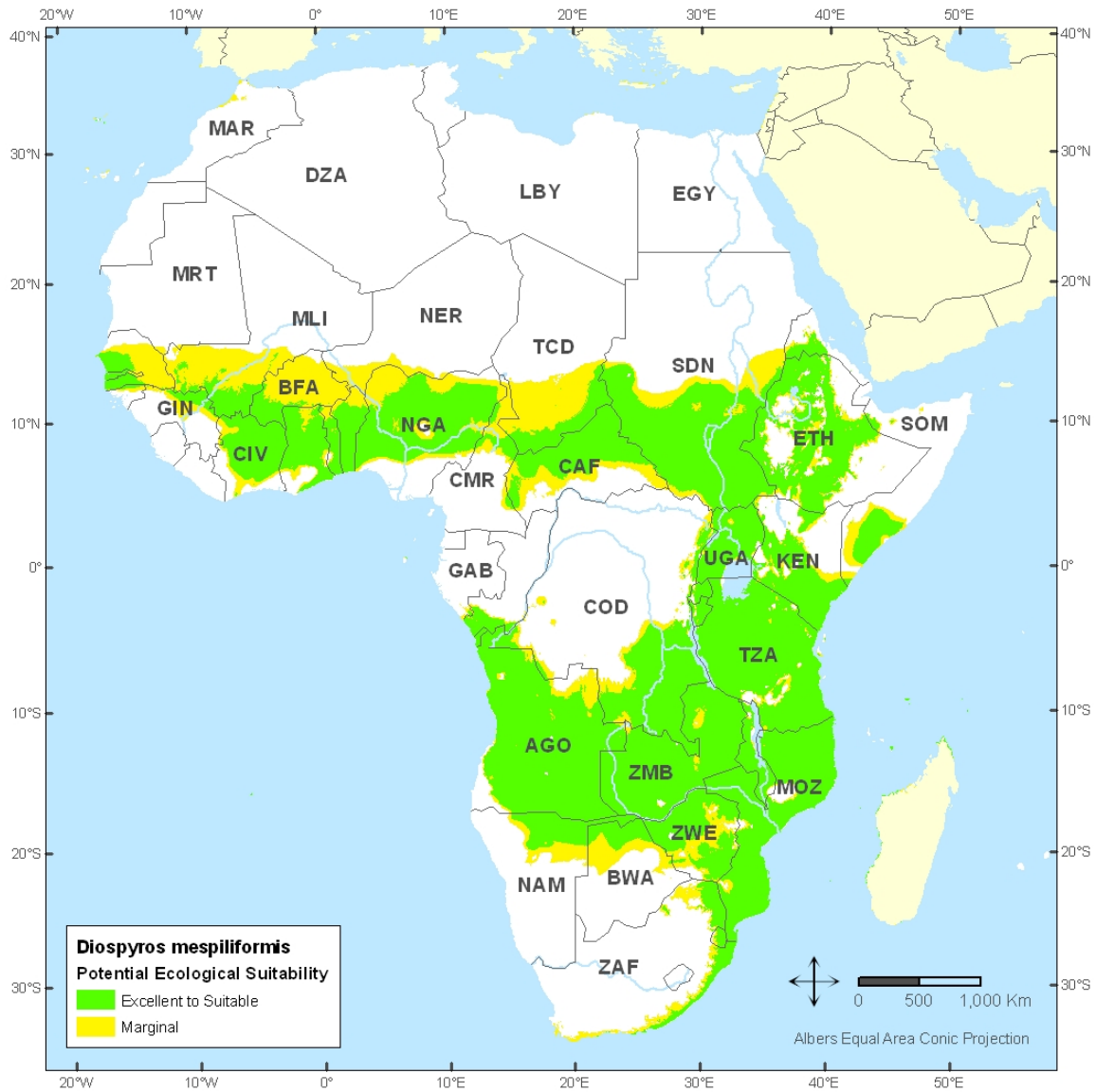


Figure 19. Taxonomic viability estimate for *Diospyros mespiliformis* based on EcoCrop modeling. The areas in green are those with Excellent to Suitable ecology. Those in yellow are Marginal to Very Marginal. The white areas have Unsuitable ecology for the growth of this species.

Table 11. Summary of ecoregions with the recorded or possible presence of mopane.

EcoCode	Ecoregion Name	Presence of <i>Mopane</i>
AT0203	Zambezi Cryptosepalum dry forests	Recorded
AT0701	Angolan Miombo woodlands	Recorded
AT0702	Angolan Mopane woodlands	Recorded
AT0704	Central Zambezi Miombo woodlands	Recorded
AT0706	Eastern Miombo woodlands	Possible
AT0709	Kalahari Acacia-Baikiaea woodlands	Recorded
AT0717	Southern Africa bushveld	Recorded
AT0719	Southern Miombo woodlands	Recorded
AT0725	Zambezi and Mopane woodlands	Recorded
AT0726	Zambezi Baikiaea woodlands	Possible
AT0902	Etosha Pan halophytics	Possible
AT0906	Zambezi coastal flooded savanna	Possible
AT0907	Zambezi flooded grasslands	Possible
AT1002	Angolan scarp savanna and woodlands	Possible
AT1310	Kaokoveld desert	Possible
AT1316	Namibian savanna woodlands	Recorded

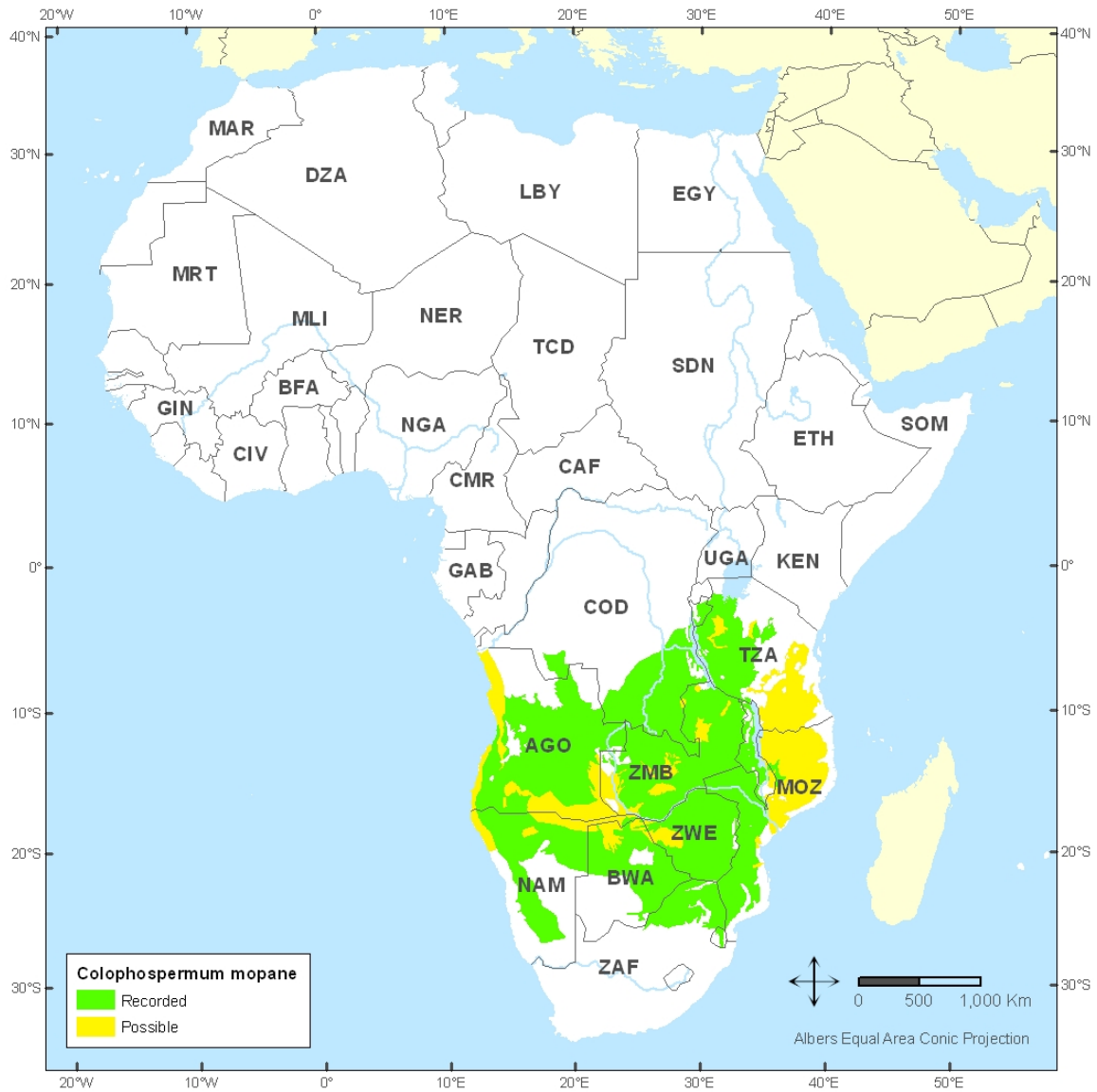


Figure 20. Taxonomic occurrence estimate based on ecoregions on the African continent with a recorded or possible presence of *Colophospermum mopane*. White areas have no recorded presence of this species.

Overall First Stage Source Attribution Estimate

A GIS intersection analysis was conducted using the four estimates: the initial environmental estimate, the initial soil estimate, the taxonomic viability estimate for *Diospyros mespiliformis* and the taxonomic occurrence estimate for *Colophospermum mopane*. Areas within continental Africa were eliminated by the following four criteria:

1. Those areas determined to be Excluded and Poor Fit from the initial environmental estimate (dark gray and light gray areas, Figure 16).
2. Those areas determined to be Excluded and Poor Fit from the initial soil estimate (dark gray and light gray areas, Figure 18).
3. Those areas determined to be Unsuitable for the taxonomic viability of *Diospyros mespiliformis* (white areas, Figure 19).
4. Those areas without the recorded presence of *Colophospermum mopane* (white areas, Figure 20)

The result is the area shown in Figure 21, which has 91.3% of the area in continental Africa eliminated.¹³ Of the 48 continental countries, three quarters have been eliminated, leaving the 12 countries shown in Table 12.

Figure 22 shows a close-up of this region, and differentiates the area into Best Fit and Next Best Fit Areas. This differentiation highlights the areas where the modeled taxonomic viability of *Diospyros mespiliformis* is ranked as Excellent to Suitable (Best Fit; green areas in Figures 19 and 22) and those where the viability is ranked as Marginal to Very Marginal (Next Best Fit; yellow areas in Figures 19 and 22).

¹³ In this GIS analysis, the total area of continental Africa is was calculated as 29,387,399 sq km, and the green region as 2,557,213 sq km.

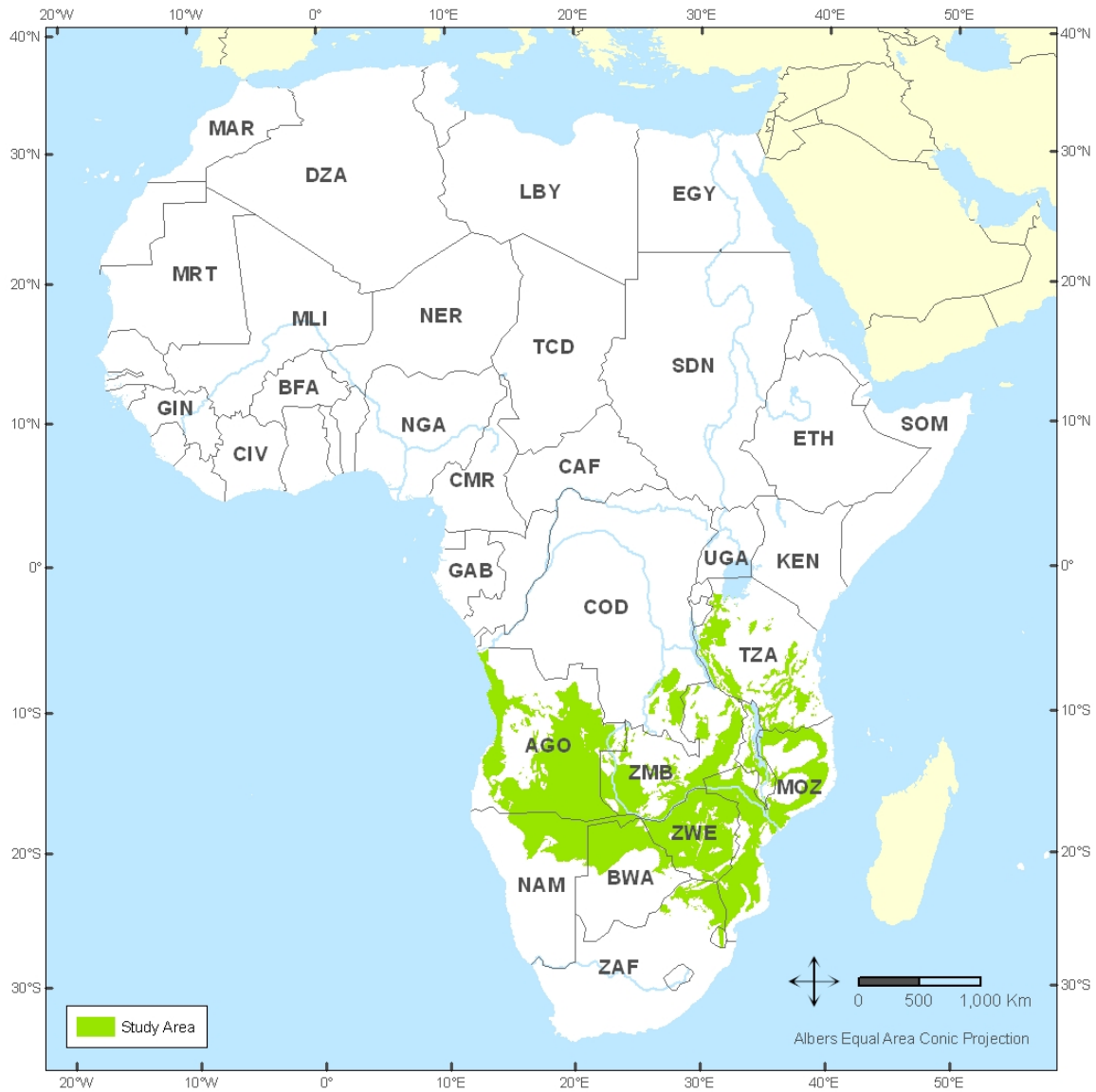


Figure 21. First stage source attribution estimate from the GIS intersection analysis combining the initial environmental estimate, the initial soil estimate, the taxonomic viability estimate for *Diospyros mespiliformis* and the taxonomic occurrence estimate for *Colophospermum mopane*.

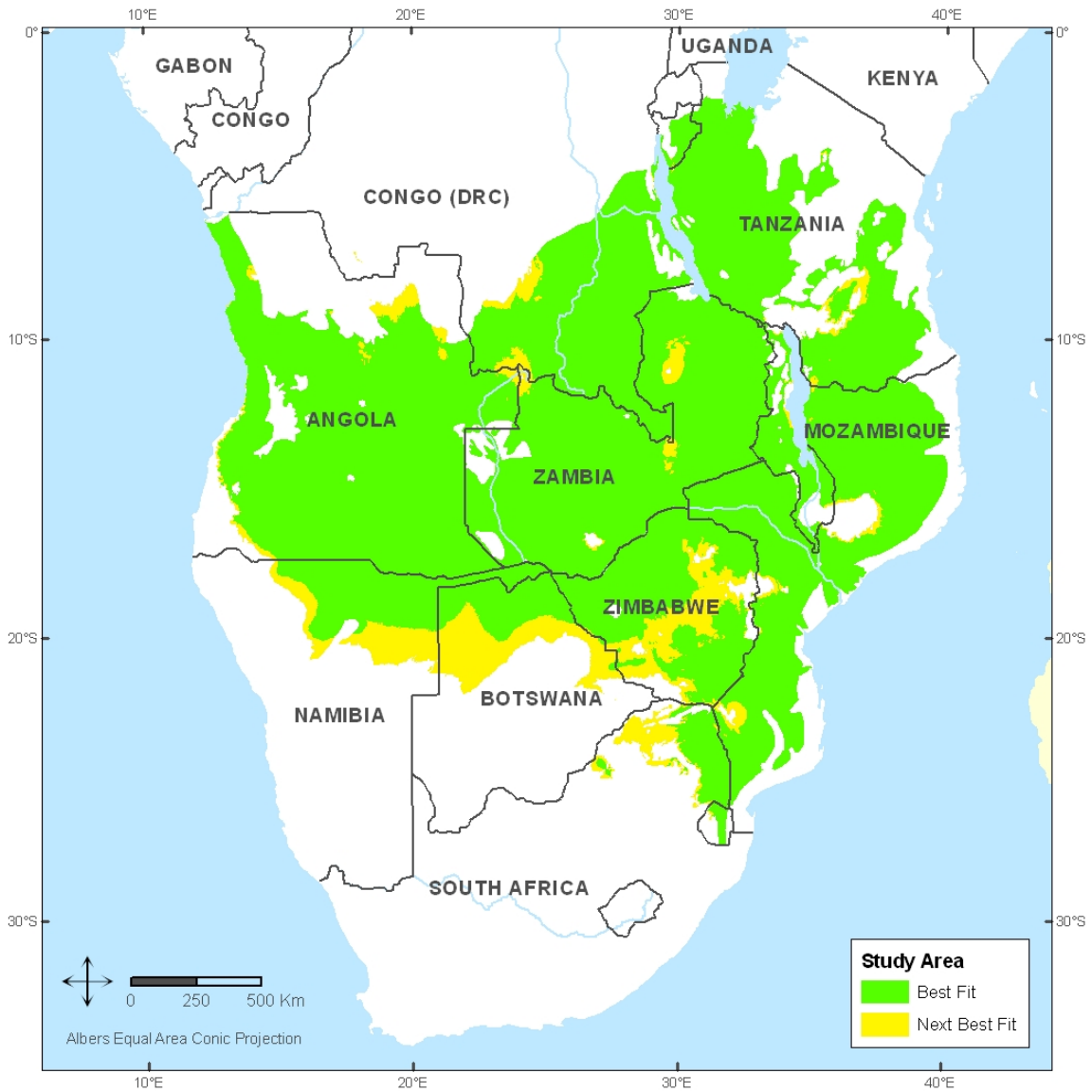


Figure 22. Close-up of the area shown in Figure 21, differentiated to show the Best Fit areas (where the taxonomic viability of *Diospyros mespiliformis* is Excellent to Suitable) and Next Best Fit areas (where the taxonomic viability of *Diospyros mespiliformis* is Marginal to Very Marginal).

Table 12. The Twelve Countries in Continental Africa Remaining in the First Stage Source Attribution Estimate, with Areas and Percentages of the Estimate (sq km)¹⁴

Country	Country Code	Total Area	Area in Estimate	Percent in Estimate	Percent of Estimate
Angola	AGO	1,252,935	698,893	55.8%	27.3%
Botswana	BWA	579,783	171,816	29.6%	6.7%
Burundi	BDI	27,098	50	0.2%	0.0%
Democratic Republic of the Congo	COD	2,336,471	64,722	2.8%	2.5%
Malawi	MWI	117,440	38,694	32.9%	1.5%
Mozambique	MOZ	793,980	436,166	54.9%	17.1%
Namibia	NAM	827,897	202,216	24.4%	7.9%
South Africa	ZAF	1,219,930	75,464	6.2%	3.0%
Swaziland	SWZ	16,823	5,692	33.8%	0.2%
Tanzania	TZA	942,536	206,308	21.9%	8.1%
Zambia	ZMB	753,941	321,909	42.7%	12.6%
Zimbabwe	ZWE	391,456	335,283	85.7%	13.1%
TOTAL AREA		9,260,289	2,557,213		

NEXT STEPS

As noted in the previous section, the result shown in Figures 21 and 22 is a First Stage Source Attribution Estimate, eliminating environments comprising approximately 91% of the area, including all areas of 36 countries. First Stage estimates enable source attribution refinements by reducing the area under investigation to one where Next Stage correspondence rankings can progress. These are based on a combination of more detailed reference information, more detailed sample characteristics, and integration with any independently obtained investigative information. In the specific case described here, the First Stage estimate, when combined with other investigative information, was sufficient to meet the case needs. One such combination is shown in Figure 23, where the areas shown in Figure 22 are reduced to those with the known and possible elephant ranges, as reported in the 2007 African Elephant Status Report.[26]

There are numerous options available for Next Stage estimates based on the sample data and variation within the First Stage estimate. For example, reference data covering the area shown in Figure 22 is shown in Figures 24 to 27 as differentiated by

¹⁴ Total Area is that of the entire country, as calculated in this GIS analysis. Area in Estimate is the calculated area, within that country, that is in the First Stage Source Attribution Estimate. Percent in Estimate is the percentage of that country’s area that is within the Estimate. Percent of Estimate is the percentage of the Estimate that is within that country.

ecosystems (ecoregions),[14] land cover,[27] soil types,[15] and geologic units.[28] From the reference data and the particles found in this sample, two of the most immediately apparent discriminating data types for the next stage are the minerals, which severely limit the possible geological units, and the close proximity of the *Zenkerella egregia* tree, whose geographical distribution is closely monitored due to its endangered species status.[29]

Based on our experience, we expect these Next Stage estimates to reduce the remaining regions on the African continent by at least another 90%, leaving less than 1%. This would take the case to a point where either another iteration of the process can be conducted (with further refinements) or where the Final Stage of source attribution is enabled.

Final Stage Source Attribution is where specific candidate sites can be indicated as hypotheses, where specific information can be provided to investigators to screen candidate sites, and where comparative testing, using traditional forensic trace evidence processes, can be employed as a test to reject or confirm specific sites.

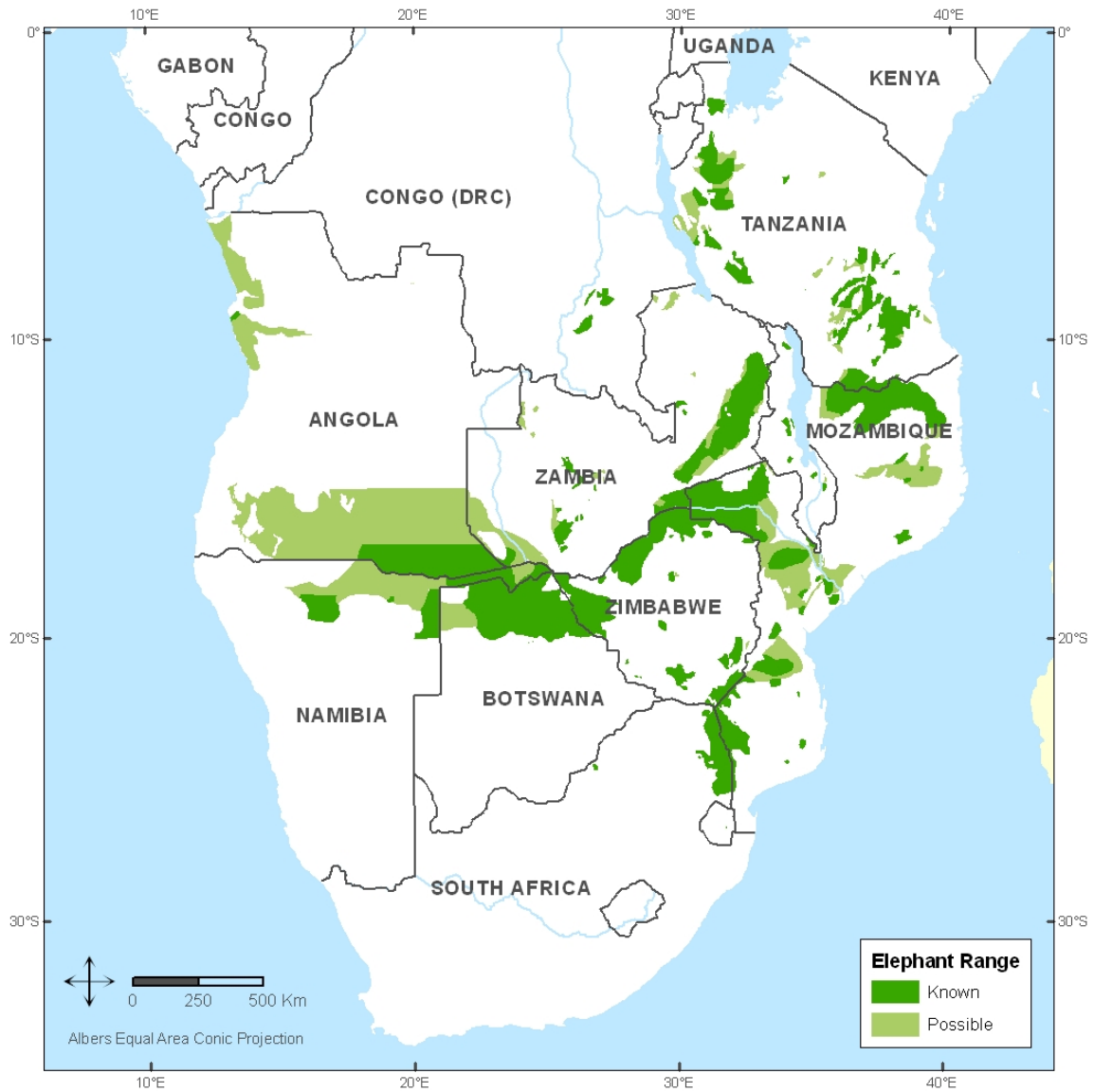
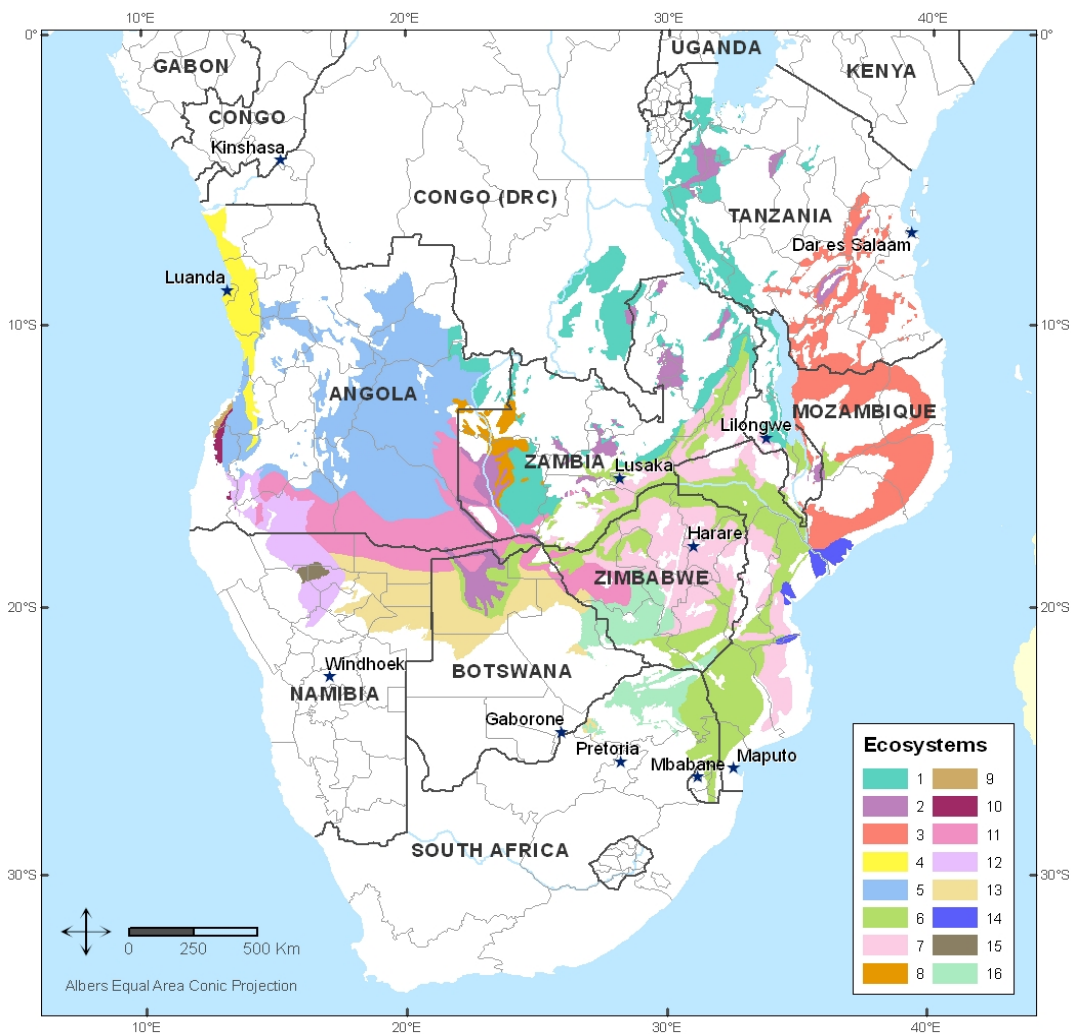


Figure 23. One of the combinations of the First Stage estimate with other investigative information: the areas within the estimate are combined with known and possible elephant ranges.



1	Central Zambezian Miombo woodlands	9	Kaokoveld desert
2	Zambezian flooded grasslands	10	Namibian savanna woodlands
3	Eastern Miombo woodlands	11	Zambezian Baikiaea woodlands
4	Angolan scarp savanna and woodlands	12	Angolan Mopane woodlands
5	Angolan Miombo woodlands	13	Kalahari Acacia-Baikiaea woodlands
6	Zambezian and Mopane woodlands	14	Zambezian coastal flooded savanna
7	Southern Miombo woodlands	15	Etosha Pan halophytics
8	Zambezian Cryptosepalum dry forests	16	Southern Africa bushveld

Figure 24. The First Stage estimate, shown differentiated by sixteen unique ecosystems (ecoregions).

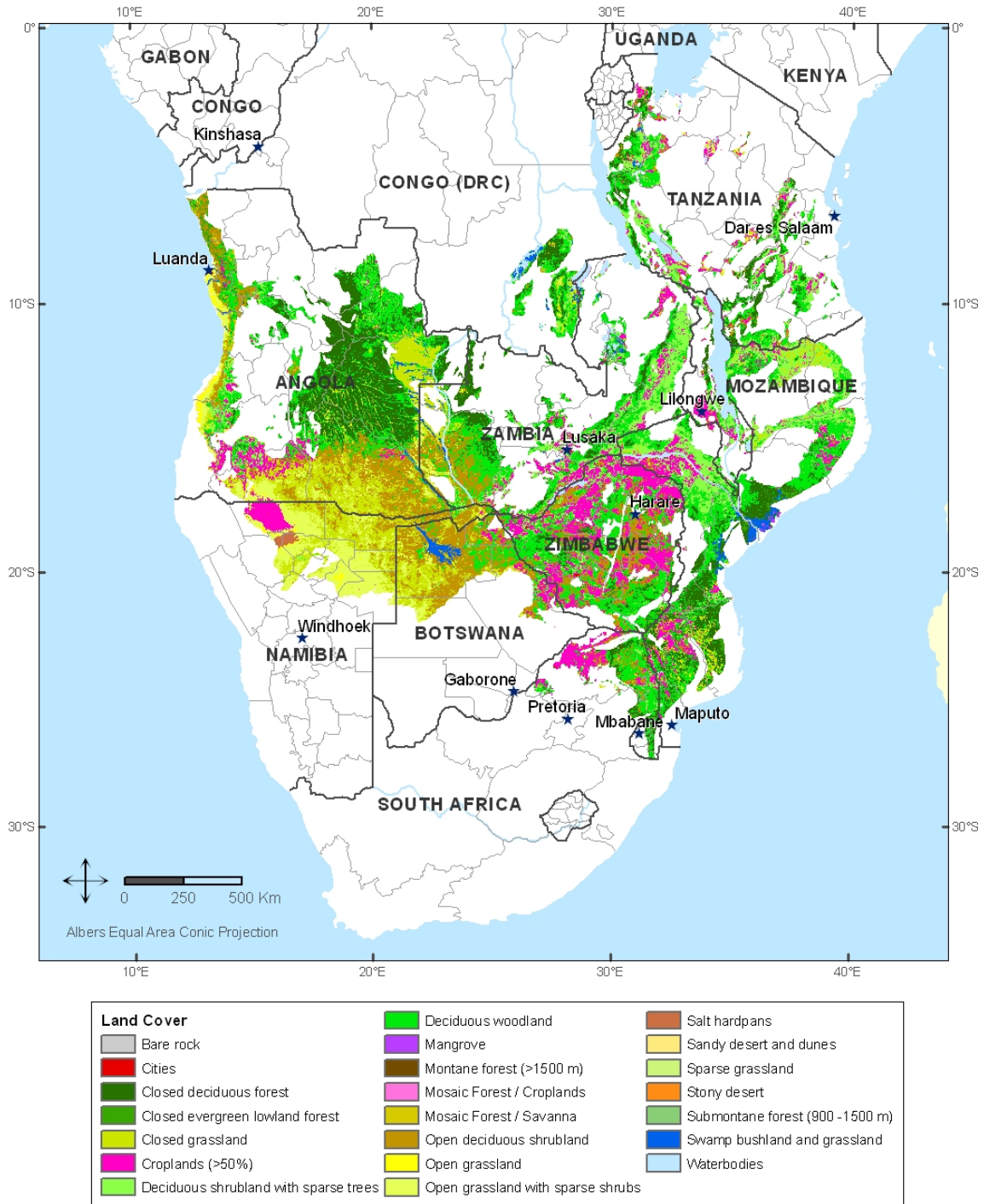
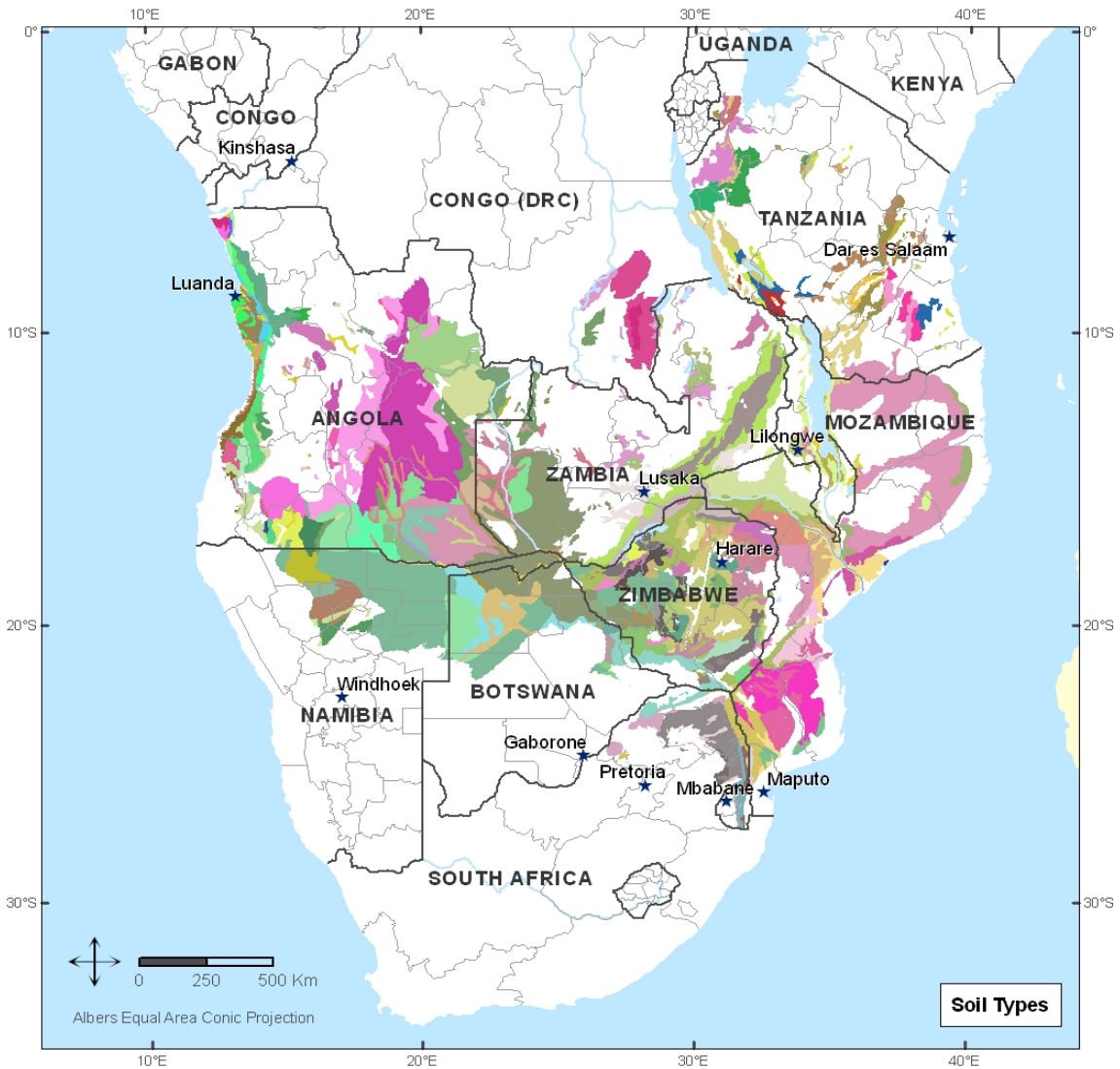


Figure 25. The First Stage estimate, shown differentiated by twenty-two land cover classes.



Soil Types															
Bc14-2bc	Ge28-1a	Je2-2/3a	Lc53-2/3a	Lf71-2ab	Lg2-1a	Qc44-1a	Rd19-1ab	Bc17-2bc	Ge29-1a	Je38-1/2a	Lc54-2/3a	Lf72-3a	Lg3-1a	Qc45-1/3a	Rd20-2c
Bc18-c	Ge30-1a	Je39-2a	Lc59-2/3a	Lf73-1a	Lk4-2ab	Qf22-1a	Re69-1a	Bc22-2/3a	Ge31-1a	Je49-2/3a	Lc64-2b	Lf74-1a	Lo41-1/2a	Qf23-1a	So13-1a
Bc7-2/3b	Ge32-2/3a	Je50-2/3a	Lc65-1/2ab	Lf76-1/2a	Lo42-1a	Qf24-1a	WATER	Bc7-2bc	Ge33-2/3a	Je51-2/3a	Lc65-1/2bc	Lf77-1/2a	Lp12-1a	Qf25-1a	We18-1/2a
Be53-1/2a	Gh7-2a	Je52-2/3a	Lf10-1a	Lf78-1/2ab	Oe3-a	Qf26-1a	We8-1/2a	Be54-2/3a	Gp5-1a	Je53-1/3a	Lf10-1ac	Lf79-2ab	Oe4-a	Qf27-1/2ab	Xh1-2ab
Be55-2/3ab	Gp6-2/3a	Je58-2/3a	Lf10-2a	Lf80-2bc	Ph5-1a	Qf28-1a	Xh15-2a	Be56-2/3ab	I	Je59-1a	Lf24-1a	Lf81-1a	Qa6-1a	Qf29-1a	Xh22-1/2ab
Be57-2/3a	I-Ao-N-c	Je60	Lf24-2a	Lf81-2a	Qc23-1a	Qf30-1a	Xh23-1/2ab	Be58-2/3b	I-Bc-V	Je7-3a	Lf29-1a	Lf81-2ac	Qc24-1a	Qf31-1ab	Xh24-ab
Bk25-2a	I-Bc-V-ac	Lc3-2ab	Lf32-2c	Lf82-1a	Qc25-1a	Qf32-1/2b	Xh25-1/2a	Bk26-2/3a	I-Bc-c	Lc3-3a	Lf33-1a	Lf83-1a	Qc26-1a	Qf34-1/2b	Xh26-1/2a
Bk28-2b	I-F-c	Lc49-2a	Lf44-1/2bc	Lf84-1a	Qc27-1a	Qf40-1a	Xh27-1/2a	Bk29-2ab	I-L-1b	Lc49-3a	Lf47-1/2ab	Lf87-2/3b	Qc28-1a	Qf15-1a	Xh28-1/2a
Bv13-3a	I-L-Q-bc	Lc5-2/3bc	Lf51-2a	Lf88-1/2bc	Qc29-1a	Qf17-1/2a	Xh29-1/2a	Bv14-2/3b	I-L-R-bc	Lc50-1/2a	Lf66-2ab	Lf88-3b	Qc32-1ab	Qf17-1a	Xk24-2ab
E16-2a	I-Lc-2bc	Lc50-1b	Lf67-2b	Lf89-1/2b	Qc33-1a	Qf12-1/2b	Zg12-1/2a	Ge25-1a	I-Lc-a	Lc50-2a	Lf68-2b	Lf90-2/3bc	Qc38-1a	Qf20-1a	
Ge26-1/2a	I-X-c	Lc51-1/2a	Lf69-ac	Lf91-3ab	Qc40-1a	Qf25-1/2a		Ge27-1a	Je1-2a	Lc52-1a	Lf70-1/2ab	Lg16-1a	Qc42-1a	Qf9-1a	

Figure 26. The First Stage estimate, shown differentiated by 172 soil types.

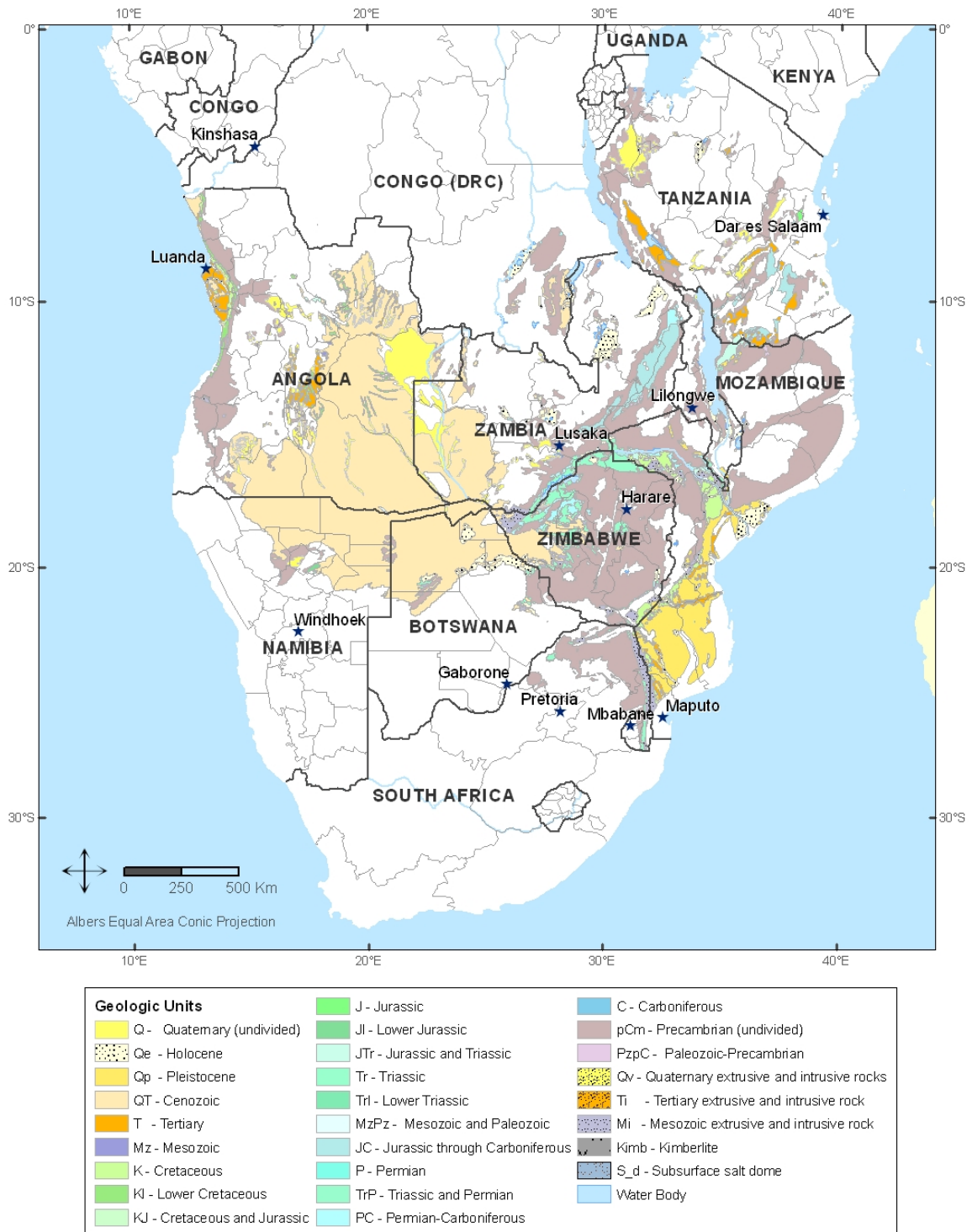


Figure 27. The First Stage estimate, shown differentiated by 27 geologic units.

DISCUSSION

The detailed analysis of dusts, when conducted with expertise appropriate for the sample, and combined with appropriate reference data, allows source attribution inferences that can resolve questions of investigative interest and allow the efficient geographical focus of investigative effort. Dusts are always present, but the specific content is highly variable, with portions that convey aspects of (for example) ecology, climate, botany, soil, geological environment, land use, geography and specific human activities. References providing the geographical distribution of these variables can be exploited using GIS analysis, and attribution hypotheses can be generated and tested for consistency with the entire dataset of particles in the sample.

In the present case, the First Stage source attribution estimate eliminated 91.3% of the geographical area under consideration, and three quarters of the countries. This, combined with other investigative information, met the international law enforcement needs of this case.

This work is an application of a new capability using Particle Combination Analysis (PCA). As this case illustrates, the PCA capability is easy to employ and does not interfere with investigation by traditional methods. For example, investigation of this case was also supported by latent print processing, x-ray examination, recovery of transfer evidence (bullet impacts, paint), elephant population genetics, entomological identifications and carbon dating.[30,31] PCA integrates with, supports and contributes to other investigation efforts, such as focusing ground investigative effort toward most likely regions or environments, and providing information on landmarks or nearby activities that can be used to screen candidate areas.

Notably for investigations involving organized crime, wildlife crimes and illegal trade, PCA enables “cross-linking” attribution among cases involving different types of evidence, endangered species and contraband. These can be linked through the analysis of combinations of particles occurring on or within the items. This is distinct from many (very useful) types of source attribution tools, such as those focused on the population genetics of a specific species,[31] the elemental and isotopic compositions of a specific foodstuff,[32] or linkages based on a library of results for the same type of contraband.[2]

Uniquely among methods for source attribution, PCA provides an iterative means to refine and test source attribution estimates. The First Stage Source Attribution Estimate, based on the combined analyses of one sub-set of particles, enables the Next Stage estimate, which can draw on a different sub-set of particles, a finer set of reference

data, or on different analytical methods used to analyze specific target particles. And, at the Final Stage of source attribution, the same samples can suggest candidate sites, guide the investigation on the ground, and test specific candidate sites.

What makes PCA work is that there are thousands of very small particles of almost unlimited type and character in the fine dusts that are present on virtually any item. The combinations are so complex that until recently there was no *practical* method to identify and interpret these combinations. The capability described here resulted from an ongoing, multi-million dollar post-9/11 federally-funded research program.

ACKNOWLEDGEMENTS

The authors gratefully acknowledge the support of the National Fish & Wildlife Forensics Laboratory and INTERPOL in general, and Kenneth Goddard, Edgard Espinoza and Peter Younger in particular, for recognizing the potential of Particle Combination Analysis in support of predictive source attribution, and for providing the opportunity to work on this case. Often there is institutional resistance to the incorporation of new methodologies, such as PCA. The RJLee Group, Inc. performed the x-ray diffraction of clay, under the direction of David Exline.

Authors' Contributions. DAS developed the PCA approach, planned its application to this case, collected samples, supervised microscopical, DNA and GIS analyses, interpreted the PCA data, and wrote the manuscript. AMB performed microscopical analysis and related interpretations. VMB performed pollen analysis and related interpretations. EAC performed environmental modeling, GIS analysis and related interpretations. MTC performed DNA analysis and related interpretations. PLS developed the PCA approach, planned its application to this case, interpreted the PCA data and revised the manuscript. All authors read and approved the manuscript.

REFERENCES

1. For example, see case reports by Wehrenburg, J, Junger, E and Schneck, B in Murray, RC. Evidence from the Earth, Mountain Press, Missoula, Montana, 2004, pp. 15-31, and cases reported by Mindenhall, DC: An unusual appearance of a common pollen type indicates the scene of the crime, *Forensic Science International* 163:236-240, 2006, and An example of the use of forensic palynology in assessing an alibi, *Journal of Forensic Sciences*, 49(2):312-316, 2004.

2. For example, see Dalpé, C, et al., Trace element analysis of rough diamond by LA-ICP-MS: A case of source discrimination?, *Journal of Forensic Sciences* 55(6):1443-1456, 2010; Waddell-Smith, RJH. A review of recent advances in impurity profiling of illicit MDMA samples, *Journal of Forensic Sciences* 52(6):1297-1304, 2007; Bartle, EK and

Watling, RJ. Provenance determination of oriental porcelain using laser ablation–inductively coupled plasma–mass spectrometry (LA–ICP–MS), *Journal of Forensic Sciences* 52(2):341–348, 2007; Casale, J, et al. Stable isotope analyses of heroin seized from the merchant vessel Pong Su, *Journal of Forensic Sciences* 51(3):603–606, 2006.

3. A number of early cases are summarized in: Palenik, S. Microscopic Evidence: The Overlooked Clue. Part 1. *The Microscope* 30:93–100, 1982; and Palenik, S. Microscopic Evidence: The Overlooked Clue. Part 2. *The Microscope* 30:163–169, 1982. Some recent examples are Lombardi, G. The contribution of Forensic Geology and Other Trace Evidence Analysis to the Investigation of the Killing of Italian Prime Minister Aldo Moro, *Journal of Forensic Sciences* 44(3):634–642, 1999; Skinner, D. Sampling Procedures in Forensic Earth Science, Lower Hutt, New Zealand: New Zealand Geological Survey, 1988; and Munter, R. A Case Study on the Application of Soil and Plant Science to Criminal Investigations: *Forensic Pedology*, 1981.

4. Deer, WA, Howie, RA, and Zussman, J. *An Introduction to the Rock Forming Minerals*, Longman Group, Ltd., London; 1975.

5. Mange, MA, and Maurer, FWH. *Heavy Minerals in Colour*, Chapman & Hall, New York, 1992.

6. Galehouse, JS. *Point Counting*, in Carver, RE (Ed.). *Procedures in Sedimentary Petrology*. Wiley Interscience, New York, NY, pp. 385–407, 1971.

7. White, TJ, Bruns, T, Lee, S, and Taylor, J. *Amplification and direct sequencing of fungal ribosomal RNA genes for phylogenetics*. In: Innis, MA, Gelfand, DH, Sninsky, JJ and White, TJ, editors. *PCR Protocols*. New York: Academic Press; 1990.

8. Environmental Systems Research Institute (ESRI). *ArcGIS 9.2 Software and Spatial Analysis Tools*; Redlands, CA; 2006.

9. Hijmans R, et al. *DIVA–GIS 5.2. A Geographic Information System for the Analysis of Biodiversity Data*; 2005. Available at: <http://www.diva-gis.org>.

10. Environmental Systems Research Institute (ESRI). *ESRI Data & Maps [CD–ROM]*; Redlands, CA; 2006.

11. World Wildlife Fund. *Afrotropic Ecoregion Profiles*. 2001. Available at: http://www.worldwildlife.org/wildworld/profiles/terrestrial_at.html.

12. World Wildlife Fund. Palearctic Ecoregion Profiles. 2001. Available at: http://www.worldwildlife.org/wildworld/profiles/terrestrial_pa.html.
13. Burgess, N, D'Amico Hales, J, Underwood, E and Dinerstein E. Terrestrial Ecoregions of Africa and Madagascar. A Conservation Assessment. Washington, DC: Island Press; 2004.
14. Olson, DM, et al. Terrestrial Ecoregions of the World: A New Map of Life on Earth, *BioScience* 51:933–938, 2001.
15. Food and Agriculture Organization of the United Nations (UN–FAO). Digital Soil Map of the World and Derived Soil Properties, Rev. 1 [CD–ROM], 2003.
16. Hijmans, RJ, et al. DIVA–GIS, Version 5.2. A Geographic Information System for the Analysis of Biodiversity Data. Manual; 2005. Available at: <http://www.diva-gis.org>.
17. Hijmans, RJ, et al. Very high resolution interpolated climate surfaces for global land areas. *International Journal of Climatology* 25:1965–1978, 2005.
18. Food and Agriculture Organization of the United Nations (UN–FAO). Data sheet: *Diospyros mespiliformis*, 2007. Retrieved from <http://ecocrop.fao.org/ecocrop/srv/en/dataSheet?id=5466>.
19. White, F, Dowsett–Lemaire, F, and Chapman, JD. Evergreen Forest Flora of Malawi, Royal Botanic Gardens, Kew, 2001.
20. Sebege, RJG and Arnberg, A. Interpretation of mopane woodlands using air photos with implications on satellite image classification. *International Journal of Applied Earth Observation and Geoinformation* 4, 119–135; 2002.
21. Hyde, MA and Wursten, B. Flora of Zimbabwe; 2008. Available at: <http://www.zimbabweflora.co.zw/index.php>
22. United States Department of Agriculture, Agricultural Research Service (USDA, ARS), National Genetic Resources Program. Germplasm Resources Information Network – (GRIN), Online Database. Available at: <http://www.ars-grin.gov/npgs>.
23. White, F. The Vegetation of Africa: A Descriptive Memoir to Accompany the Unesco / AETFAT / UNSO Vegetation Map of Africa. UNESCO, Natural Resource Research 20:1–356, 1983.

24. Aluka. Flora of West Tropical Africa. Online Database. Available at: <http://www.aluka.org>.
25. Kew Gardens, Flora Zambesiaca. Online Database. Available at: <http://apps.kew.org/efloras>.
26. Blanc, JJ, et al. African Elephant Status Report 2007: An Update from the African Elephant Database. Available at: <http://www.african-elephant.org/aed/aesr2007.html>
27. Mayaux, P, Bartholomé, E, Fritz, S and Belward, A. A new land-cover map of Africa for the year 2000. *Journal of Biogeography* 31: 861–877, 2004.
28. Persits, FM, et al. Map showing geology, oil and gas fields and geologic provinces of Africa: U.S. Geological Survey Open File Report 97–470A, version 2.0. CD-ROM, US Geological Survey, Denver, CO, 2002. (Also available at <http://pubs.usgs.gov/of/1997/ofr-97-470/OF97-470A/index.html>).
29. International Union for Conservation of Nature 2010. IUCN Red List of Threatened Species. Version 2010.4. <www.iucnredlist.org>. Downloaded on 10 February 2011.
30. Goddard, K. CSI in a Box. Presented at INTERPOL, 6th International Conference on Environmental Crime, Lyons, France, October 13–17, 2008.
31. Wasser, SK, Clark, B, Laurie, C, and Weir, B. The Illegal Ivory Trade and Organized Crime. Presented at the April 21, 2010. For the techniques and approach, see Wasser, SK, Clark, B, and Laurie, C. The Ivory Trail. *Scientific American* July, 2009, pp. 68–76.
32. Some examples are: Ariyama, K, et al. Determination of the geographic origin of onions between three main production areas in Japan and other countries by mineral composition. *Journal of Agricultural and Food Chemistry* 55(2):347–354, 2007; Di Giacomo, F, Del Signore, A, and Giaccio, M. Determining the geographic origin of potatoes using mineral and trace element content. *Journal of Agricultural and Food Chemistry* 55(3):860–866, 2007; Crittenden, RG, et al. Determining the geographic origin of milk in Australasia using multi-element stable isotope ratio analysis. *International Dairy Journal* 17(5):421–428, 2007; Rodrigues, CI, et al. Stable isotope analysis for green coffee bean: A possible method for geographic origin discrimination. *Journal of Food Composition and Analysis* 22(5):463–471, 2009.